DOCTORAL DISSERTATION

Development of Liposomal Agents for Physically-Induced Selective Cytotoxicity toward Tumor Cells

Shoji Tachikawa

2015

Graduate Course in Life Science
Graduate School of Science
Gakushuin University

Dissertation Examiner
Professor Fumio Hanaoka
Graduate School of Science
Gakushuin University

Contents

List of Publication

1. Tachikawa, S., Miyoshi, T., Koganei, H., El-Zaria, M. E., Viñas, C., Suzuki, M., Ono, K., Nakamura, H. (2014) Spermidinium *closo*-dodecaborate-encapsulating liposomes as efficient boron delivery vehicles for neutron capture therapy, *Chem. Comm.*, 50, 12325-12328.

2. Tachikawa, S., El-Zaria, M. E., Inomata, R., Sato, S., Nakamura, H. (2014) Synthesis of protoporphyrin–lipids and biological evaluation of micelles and liposomes. *Bioorganic & Medicinal Chemistry*. 22(17), 4745-4751.

3. 立川将士、中村浩之、がん光線力学療法のための DDS 薬剤の開発＝ポルフィリン脂質の開発とナノキャリアへの応用＝、光アライアンス、特集 : 悪性新生物で効果的に活用される光医用技術、2014、9 月、12-16

Other Publication

4. Nakamura, H., Ueda, N., Ban, H. S., Ueno, M., Tachikawa, S. (2012) Design and synthesis of fluorescence-labeled *closo*-dodecaboratelipid:Its liposome formation in vivo imaging targeting to tumor for boron neutroncapture therapy, *Org. Biomol. Chem*., **10**, 1374-1380.

5. Bialek-Pietras, M., Olejniczak, A. B., Tachikawa, S., Nakamura, H., Lesnikowski, Z. J. (2013) Towards new boron carriers for boron neutron capture therapy: metallacarborones and their nucleoside conjugates, *Biooraganic & Medicinal Chemistry*, 21, 1136-1142.

6. Koganei, H., Ueno, M., Tachikawa, S., Tasaki, L., Ban, H. S., Suzuki, M., Shiraisi, K., Kawano, K., Yokoyama, M., Maitani, T., Ono, K., Nakamura, H. (2013) Development of High Boron Content Liposomes and Their Promising Antitumor Effect for Neutron Capture Therapy of cancer, *Bioconjugate Chem.*, 24, 124-132.

7. Yamauchi, M., Honda, N., Hazama, H., Tachikawa, S., Nakamura, H., Kaneda, Y., Awazu, K. (2014) A novel photodynamic therapy for drug-resistant prostate cancer cells using porphyrus envelope as a novel photosensitizer, *Photodiagnosis and Photodynamic Therapy*, 11, 48-54.

8. Verdia-Baguena, C., Alcaraz, A., Aguilella, V. M., Cioran, A. M., Tachikawa, S., Nakamura, H., Teixidor, F., Viñas, C. (2014) Amphiphilic COSAN and 12-COSAN crossing synthetic lipid membranes: planar bilayers and liposomes, *Chem. Comm.*, 50, 6700-6703.

9. 上田記子、小金井逸人、上野学、立川将士、鈴木実、小野公二、中村浩之 (2012) 蛍光標識ホウ素脂質の開発とリポソーム化による細胞内イメージング **Progress in Drug Delivery System XXI,** 68-73.

Patent

「ホウ素１０同位体を含むホウ素化合物を内封したリポソーム」
立川将士、中村浩之、2011 年　特願 2011-128379

Abbreviation

conc.	concentration
DMSO	dimethylsulfoxide
EDTA	ethylenediaminetetraacetic acid
ESI	electric spray ionization
FBS	fetal bovine serum
IC50	median inhibitory concentration
IR	infrared spectroscopy
Min.	minute(s)
MS	mass spectra
MTT	3-(4,5-dimethylthiazol-2-yl)-2,5-diphenyl tetrazolium bromide
NMR	nuclear magnetic resonance
PBS	phosphate-buffered saline
SEM	standard error of the mean
TLC	thin layer chromatography
Triton X-100	octylphenolpoly(ethyleneglycolether)
UV	ultraviolet

Introduction

1.1. Cancer therapy

Cancer has become one of the major diseases with high rate of crisis. [1] In general, surgery, chemotherapy, and radiotherapy as three major treatments are widely used for cancer patients. The cancer cells in the human body are unable to remove completely at all time by surgery, chemotherapy and radiotherapy. These therapies have limited specificity to cancer cells along with side effects to normal tissues.

Three major treatments for cancer therapy

- Surgery: directly removal of the tumor from human body
- Chemotherapy: the use of medicines or drugs to kill cancer cells
- Radiation therapy: the use of high-energy particles or waves to destroy cancer cells

However, cancer treatment has dramatically changed for the purpose of reducing the side effects. Development of a noninvasive therapy is now emerging requirement in terms of quality of life (QOL) for cancer patients. In this regards, much attention has been focused on BNCT (Boron Neutron Capture Therapy), PDT (Photodynamic Therapy) and Heavy ion radiotherapy as a next generation therapy of cancers. In this thesis, I focused on BNCT and PDT and studied the development of new therapeutic agents based on the technology of liposomal drug delivery system.

Noninvasive treatment for cancer

- BNCT: radiation therapy using nonradioactive ^{10}B and thermal neutrons
- PDT: the use of photosensitizer and light induced ROS to kill cancer cell
- Heavy ion radiotherapy: the use of massive particles such as carbon ions

1.2. DDS (Drug Delivery System)

Drug delivery systems (DDS) are systems for the delivery of drugs to target sites of pharmacological actions. The technologies of DDS modify drug release, absorption, distribution and elimination for the benefit of improving product efficacy and safety, as well as patient convenience and compliance. DDS carrier having these functions such as liposomes, micelles, and nanogel particles can be designed to improve the pharmacological and therapeutic properties of drugs administered parenterally. The clinical applications of particulate DDS carrier have been overcome many of the early problems, and several DDS formulations of anticancer and antifungal drugs now approved for clinical use. [3]

1.3. Liposome

A liposome is a spherical vesicle like biomembrane composed of a lamellar phaselipid bilayer. [4] Liposomes as DDS carrier have three major advantages accrued from their demonstrated ability: (i) to reduce serious side effects and undesirably absorption of drug, (ii) to enhance significantly the accumulation of drug into liposome, (iii) to encapsulate a various drug of hydrophilic and hydrophobic. Liposomes are also non-toxic, biodegradable and are readily prepared on a large scale. Therefore, the liposome can be used as drug carriers for improving the delivery of therapeutic agents. Due to new developments in liposome technology, several liposome-based drug formulations are currently in clinical trial, and recently some of them, such as DOXIL®(Janssen Pharma), Ambisome®(Sumitomo Dainippon Pharma), Visudyne® (Novartis Pharma) have been approved for clinical use. [5] Reformulation of drugs in liposomes has provided an opportunity to enhance the therapeutic indices of various agents mainly through alteration in their biodistribution.

1.4. EPR effect (Enhanced Permeability and Retention)

The enhanced permeability and retention (EPR) effect have the property that tend to accumulate a certain size particles as liposomes in tumor tissue. [6] Therefore, the EPR effect is important for liposomal drug delivery to cancer tissue.
In this thesis, I focused on a liposome as a drug delivery system and developed liposomal agents for BNCT and PDT.

1.5. Referrence

[1] M. Ferrari, Cancer nanotechnology: opportunities and challenges, *Nat. Rev. Cancer.*5 (2005) 161.

[2] D. Peer, J.M. Karp, S. Hong, O.C. Farokhzad, R. Margalit, R. Langer, Nanocarriers as an emerging platform for cancer therapy, *Nat. Nanotechnol.*2 (2007) 751.

[3] M.A. Theresa, R.C. Pieter, Drug Delivery Systems: Entering the Mainstream, *science*, *19* (2004) 1818-1822

[4] A.D. Bangham, R.W. Horne, Negativestaining of phospholipids and their structural modification by surface-active a gents as observed in the electron microscope. *J Mol Biol*. *8* (1964) 660-668.

[5] M.L. Immordino, F. Dosio, L. Cattel, Stealth liposomes: review of the basic science, rationale, and clinical applications, existing and potential, *Int. J. Nanomedicine*. *1* (2006) 297-315.

[6] Y. Matsumura, H. Maeda, A new concept for macromolecular therapeutics in cancer chemotherapy: mechanism of tumoritropic accumulation of proteins and the antitumor agent smancs, *Cancer Res., 46* (1986) 6387-6392.

Boron-Encapsulating Liposomes and Their Promising BNCT Effects in Mice

2.1. Introduction

The development of minimally invasive cancer therapy is one of the most pressing issues at hand to improve the quality of life of cancer patients receiving treatment. Boron neutron capture therapy (BNCT) has been attracting growing interest as a candidate therapy for this purpose. [1-3] BNCT is a bimodal approach to cancer treatment. It is reliant on the selective uptake and/or retention of sensitizing ^{10}B molecules by tumor cells and the activation of those sensitizers by thermal neutrons from an external radiation source. The nuclear reaction of essentially nontoxic ^{10}B species and low-energy thermal neutrons (0.025 eV) yields high linear energy transfer (LET) particles, ^{7}Li nuclei and ^{4}He (α-particles), bearing energy of approximately 2.4 MeV, which travel a distance within one cell diameter (approximately 5−9 μm) with destroying cells. Therefore, tumor cells can be selectively killed by thermal neutron irradiation if ^{10}B molecules are selectively delivered to them. [4] Mercaptoundecahydrododecaborate ($Na_2[B_{12}H_{11}SH]$; Na_2BSH) [5-7] and L-*p*-boronophenylalanine (L-BPA) [8, 9] have been used for the treatment of brain tumor and melanoma, respectively, for BNCT. L-BPA has been widely used for the treatment of not only melanoma but also brain tumor [10] and head and neck cancer [11-13] because tumor cells can take in it selectively through an amino acid transporter. [14-17] The accelerator-based BNCT with the use of L-BPA is now undergoing phase I clinical study for the treatment of brain tumor patients in Japan. [18,19]

The successful treatment of cancer patients by BNCT relies on the selective delivery of ^{10}B to tumor cells and its high accumulation therein. In general, 20–35 μg ^{10}B/g tumor tissue is required to realize fatal tumor cell damage while keeping ^{10}B concentrations low in surrounding normal tissues and blood to minimize damage to those tissues. Although Na_2BSH and L-BPA have been utilized for BNCT, effective concentrations of ^{10}B are not observed in some patients. Therefore, the development of new ^{10}B carriers is still an important task to widen the alternatives for cancer treatment in BNCT.

In recent years, a liposome as DDS (Drug Delivery System) carrier has attracted attention as one of the efficient boron delivery systems in BNCT. The liposomal ^{10}B carriers can transport their contents to various tumors in a manner that is essentially independent of

their contents by means of the enhanced permeability and retention (EPR) effect [20, 21] that relies on the abnormal architectures of newly formed tumoral blood vessels. [22] Various ^{10}B-encapsulating liposomes have been developed, including passive targeting liposomes and tumor-specific ligand-conjugating active targeting liposomes. [23, 24] In the last decade, several efficient *in vivo* BNCTs have been demonstrated. Maruyama and co-workers developed transferrin-conjugating liposomes for active targeting. [25] Na_2BSH was used as the ^{10}B molecule and encapsulated in the liposomes. Although they succeeded in completely inhibiting tumor growth in mice after neutron irradiation, the concentration of ^{10}B encapsulated in liposomes inner side was limited due to osmotic reasons. Approximately 743 mg/kg of 1,2-distearoyl-sn-glycero-3-phosphocholine (DSPC) is necessary to administer a boron dose of 35 mg [^{10}B]/kg in this case. This total liposome dose is quite high for clinical use. The pre-injection of liposomes at a high dose was conventionally done for targeting via saturation of the liver's scavenging capacity. The injection of such a high liposome dose, however, may be toxic to liver because the liver's normal scavenging function is impaired. Therefore, the development of high ^{10}B content liposomes is necessary for clinical use. Hawthorne and coworkers developed liposomes incorporating $Na_3[1\text{-}(2\text{-}B_{10}H_9)\text{-}2\text{-}NH_3B_{10}H_8]$ in the internal aqueous interior and K[*nido*-7-$CH_3(CH_2)_{15}$-7,8-$C_2B_9H_{11}$] in the bilayer membrane. [26] Biodistribution studies indicated that two identical injections given 24 h apart resulted in tumor boron levels exceeding 67 μg/g tumor at 54 h. Significant suppression of tumor growth was observed in mice that received a double injection (a total of 35 mg [^{10}B]/kg) and neutron irradiation (1.6 x 10^{12} neutrons/cm^2), and an approximately 25% increase in tumor volume compared to that of untreated controls was noted at 14 days post irradiation. [27] We previously developed Na_2BSH-encapsulating 10% distearoyl boron lipid (DSBL) [28,29] liposomes having high boron content (boron/phosphorus (B/P) ratio: 2.6), which enabled us to prepare liposome solution containing 5,000 ppm boron. The Na_2BSH-encapsulating 10% DSBL liposomes displayed excellent boron delivery to tumor: boron concentrations reached 174, 93, and 32 ppm at doses of 50, 30, and 15 mg B/kg, respectively. Significant antitumor effect was observed in mice that received a single injection even at the dose of 15 mg [B[/kg; the tumor completely disappeared three weeks after thermal neutron irradiation ((1.5−1.8) x 10^{12} neutrons/cm^2), revealing that the total

amount of DSPC necessary for administration can be reduced to approximately 147 mg/kg, which is less than one-fifth of the amount used in Na_2BSH-encapsulating liposomes. [30]

In this work, I studied the effects of the counter cations of boron clusters for the liposome formation. I was able to develop high boron content liposomes for BNCT by overcoming osmotic pressure limitations.

2.2. Results

2.2.1. Synthesis and cytotoxicity of sodium closo-dodecaborates

$Na[B_{12}H_{11}NH_3]$ and $Na_2[B_{12}H_{11}OH]$ were synthesized from $Na_2[B_{12}H_{12}]$ according to procedures modified from those in the literature, [31, 33] as shown in Scheme 1. $Na_2[B_{12}H_{12}]$ (**1**) was treated with $[NH_4]_2[SO_4]$ in the presence of Me_4NCl in water to give $[NMe_4][B_{12}H_{11}NH_3]$ (**2**) in 80% yield, and $[NMe_4][B_{12}H_{11}NH_3]$ was transformed into its sodium form $Na[B_{12}H_{11}NH_3]$ (**3**) by an ion-exchange resin (Amberlite IR120). On the other hand, $Na_2[B_{12}H_{12}]$ was treated with H_2SO_4 followed by $CaCO_3$ in the presence of $[PMePh_3]Br$ to afford $[MePPh_3]_2[B_{12}H_{11}OH]$ (**4**) in 50% yield. Ion exchange of $[PMePh_3]_2[B_{12}H_{11}OH]$ with Amberlite IR120 gave $Na_2[B_{12}H_{11}OH]$ (**5**) in 85% yield. The cytotoxicity of Na_2BSH, $Na[B_{12}H_{11}NH_3]$, $Na_2[B_{12}H_{11}OH]$ toward mouse colon 26 cells is shown as the concentration necessary to inhibit cell growth by 50% (GI_{50}) in Table 1. These four boron clusters are relatively non-toxic and GI_{50} values are higher than 2.4 mM (252 ppm B). $Na[B_{12}H_{11}NH_3]$ displayed the lowest cytotoxicity among the four clusters; its GI_{50} is 32.9 mM (3948 ppm B). Since Na_2BSH has been utilized for the clinical treatment of brain tumor in BNCT, [34] the other three clusters, $Na[B_{12}H_{11}NH_3]$, $Na_2[B_{12}H_{11}OH]$, and $Na_2[B_{12}H_{12}]$, are also considered to have sufficiently low toxicity for clinical use.

Table 1. Growth inhibition of colon 26 cells

	GI_{50} (mM)	(ppm B)
Na_2BSH	2.1±0.2	252
$Na[B_{12}H_{11}NH_3]$	32.9±0.6	3948
$Na_2[B_{12}H_{11}OH]$	7.7±0.6	924
$Na_2[B_{12}H_{12}]$	5.1±0.8	612

2.2.2. Physical characterization of liposomes containing closo-dodecaborates associated with sodium and various ammonium cations

Liposomes containing various *closo*-dodecaborates were prepared from DSPC, cholesterol, and DSPE-PEG2000 by the reverse phase evapolation method (REV) method, and particle sizes and zeta potentials were measured with an electrophoretic light scattering spectrophotometer. B/P ratios were calculated from data obtained by the simultaneous measurement of boron and phosphorus concentrations by ICP-AES. We prepared liposomes (approximately 100 nm in diameter) containing various sodium *closo*-dodecaborates and examined the effects of functional groups on the liposome formation. The results are summarized in Table 2. Liposome containing Na_2BSH, which was prepared from DSPC, cholesterol, and DSPE-PEG2000 (1: 1: 0.11, molar ratio) according to the reported conditions, [25, 30] showed the zeta potential of -27.3 ± 13.4 mV. The final boron and phosphorus concentrations of the liposome solution were 3,438 ± 2.0 and 2,864 ±18.3 ppm, respectively, and B/P ratio was 1.2. Liposome yield was 58.2% based on the total phospholipids used in the preparation. Zeta potentials of liposomes encapsulating Na_2BSH, $Na[B_{12}H_{11}NH_3]$, $Na_2[B_{12}H_{11}OH]$, and $Na_2[B_{12}H_{12}]$ were similar with a range of -29.9~-24.9 (entries 1-4). The B/P ratio of liposome containing $Na[B_{12}H_{11}NH_3]$ was 2.2 (entry 2), which was slightly higher than those of liposomes containing Na_2BSH, $Na_2[B_{12}H_{11}OH]$, and $Na_2[B_{12}H_{12}]$ (1.2~1.6, entries 1, 3, and 4). Then, we examined the effects of counter cations on liposome formation. The B/P ratio of liposome containing the *n*-$C_3H_7NH_3^+$ salt of BSH was 1.3, which was similar to that of liposome containing Na_2BSH (entry 1 *vs.* 5). In the case of liposome containing the $H_3N^+C_4H_8NH_3^+$ salt of BSH, B/P ratio was increased to 2.6 and boron concentration was 4,711 ppm; those values were higher than those of liposome containing $Na[B_{12}H_{11}NH_3]$ (entry 2 vs. 6). Interestingly, the B/P ratio dramatically increased to 3.4 when spd cation was employed (entry 7). In addition, liposome yield was markedly increased to 97.9%, zeta potential was elevated to -14.7 mV, and final boron concentration of the liposome solution reached 13,867 ppm. In contrast, the B/P ratio of

liposome containing spd-BSH dropped to 2.7, although liposome yield was still high (86.5% yield) and final boron concentration of the liposome solution was high at 9,759 ppm (entry 8). Liposome containing spd-[$B_{12}H_{11}NH_3$] showed the highest B/P ratio (3.5); boron concentration of the liposome solution reached 13,790 ppm and liposome yield was 95.4% (entry 9).

Table 2. Physical characteristics of liposomes containing *closo*-dodecaborates associated with sodium and various ammonium cations[a]

Entry	Boron cluster	Particle size (nm)	Zeta potential (mV)[b]	Boron conc. (ppm)[b,c]	Phosphorus conc. (ppm)[b]	B/P ratio (%)	Liposome yield (%)[d]
1	Na_2BSH	102±0.2	-27.3±13.4	3,438 ±2.0	2864±18.3	1.2	58.2
2	$Na[B_{12}H_{11}NH_3]$	105±1.0	-24.9±16.6	4,072 ±22.8	1835±38.5	2.2	44.3
3	$Na_2[B_{12}H_{11}OH]$	110±1.2	-29.9±85.5	2,635 ±184.2	1600±99.0	1.5	38.7
4	$Na_2[B_{12}H_{12}]$	98±0.7	-25.8±11.9	3,133 ±10.3	1932±13.3	1.6	46.7
5	$(n\text{-}C_3H_7NH_3)_2BSH$	110±0.7	-23.6±19.1	2,874 ±47.7	2224.8±15.8	1.3	53.8
6	$(H_3NC_4H_8NH_3)BSH$	116±0.7	-25.4±18.3	4,711 ±17.4	1833.3±43.4	2.6	44.3
7	spd-BSH	99±0.2	-14.7±14.1	13,867 ±185.8	4046.0±18.3	3.4	97.9
8	(sperminium)BSH	101.2±1.7	-5.4±11.5	9,759 ±139.6	3558.8±44.5	2.7	86.5
9	spd-$[B_{12}H_{11}NH_3]$	100±0.2	-10.7±21.7	13,970 ±216.5	3943.0±43.4	3.5	95.4

[a]In all case, liposomes were prepared from DSPC, cholesterol, and DSPE-PEG2000 (1: 1: 0.11, molar ratio) by the REV method. Liposome diameter was approximately 100 nm as measured with an extrusion apparatus.

[b]Data are expressed as means ± standard deviation.

[c]Boron and phosphorus concentrations were calculated for 1.5 mL of liposome solution.

[d]Liposome yields were calculated from the phosphorus concentration of liposome solution based on the total phospholipids used in preparation.

2.2.3. Effect of spd cations on formation of BSH-encapsulating liposomes

The osmotic pressures of various spd cation concentrations with/without $[BSH]^{2-}$ in solutions were measured by the osmometer (Advanced™ Osmometer Model 3D3). The osmotic pressures of the solutions were dependent on the total ion concentrations of both spd cation and $[BSH]^{2-}$ (data not shown). For instance, the osmotic pressures of Na_2BSH solution (125 mM) and spd chloride solution (125 mM) were 305 and 355 mOsm/kg H_2O, respectively, whereas that of a mixed solution of Na_2BSH and spd chloride (125 mM of each) was 592 mOsm/kg H_2O. Next, the viscosity of various spd cation concentrations with/without $[B_{12}H_{12}]^{2-}$ in solutions were measured by the viscometer (DV-1 + Viscometer, Brookfield, USA). The viscosities of water and saline (approximately 125 mM NaCl solution) were 1.23 and 1.28, respectively, whereas those of $Na_2[B_{12}H_{12}]$, spd cation, and spd-$[B_{12}H_{12}]$ solutions at 125 and 250 mM ranged from 1.23 to 1.29. The results indicate that the spd cation of $[B_{12}H_{12}]^{2-}$ does not affect the viscosity of internal aqueous solution of liposomes, although the osmotic pressure of the internal aqueous solution of liposomes is strongly dependent on the concentration of the contents. We measured liposome yields and B/P ratios under the condition of various ratios of BSH to spd cations (Na_2BSH: [spermidine + HCl] = 1: X, X = 0, 0.25, 0.5, 1, and 2). As shown in Figure 1, B/P ratio reached a maximum of 3.4 when the BSH: spd ratio was 1:1. Liposome yields showed a similar tendency to B/P ratios. The highest liposome yield was observed at the BSH to spd cation ratio of 1:1.

Table 3. Viscosities of sodium and spermidinium cations of $[B_{12}H_{12}]^{2-}$ solution

Sample	Viscosity (cp)
water	1.23
$Na_2[B_{12}H_{12}]$ (125 mM)	1.27 - 1.29
$Na_2[B_{12}H_{12}]$ (250 mM)	1.23
Spermidine (125 mM)	1.23
Spermidine (250 mM)	1.23 - 1.25
spd-$[B_{12}H_{12}]$ (125 mM)	1.23 - 1.24
spd-$[B_{12}H_{12}]$ (250 mM)	1.22 - 1.24
NaCl solution (125 mM)	1.28

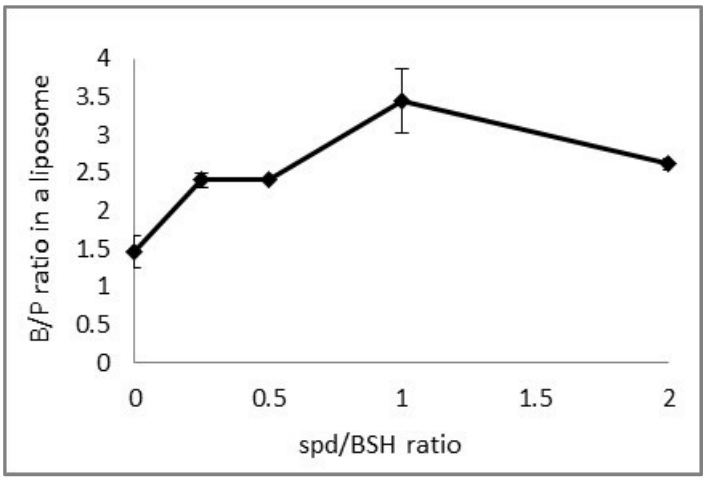

Figure 1. Effect of amount of spd cation on B/P ratio of liposomes encapsulated spd-BSH. Boron/phosphorus (B/P) ratios of $(spd)_x$-*closo*-dodecaborate-encapsulating liposomes are shown in the vertical axis.

2.2.4. Effect of spd cations on stability of closo-dodecaborate-encapsulating liposomes

The stability of various *closo*-dodecaborate-encapsulating liposomes in saline was analyzed by measuring the time-dependent B/P ratios of liposome solutions. The results are shown in Figure 2. In the case of Na_2BSH-encapsulating liposomes, B/P ratio decreased to 1.2, 14 days after the preparation of liposomes. On the other hand, the B/P ratios of liposomes containing spd-BSH and spd-$B_{12}H_{11}NH_3$ were higher than 2.5, 14 days after liposome preparation.

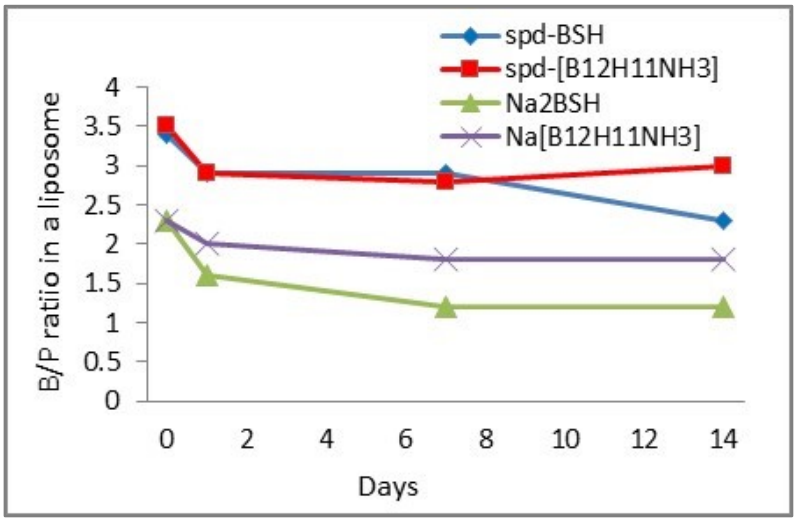

Figure 2. Time-dependent leakage of encapsulated *closo*-dodecaborates from liposomes in saline. Boron/phosphorus (B/P) ratios of spd- and sodium-*closo*-dodecaborate-encapsulating liposomes are shown in the vertical axis. (◆, spd-BSH; ■, spd-[$B_{12}H_{11}NH_3$]; ▲, Na_2BSH; ×, Na[$B_{12}H_{11}NH_3$])

2.2.5. Transmission electron microscopy analysis

Transmission electron microscopy (TEM) analysis of spd-BSH-encapsulating liposomes (left) and Na_2BSH-encapsulating liposomes (right) was carried out with Cryo-TEM. As shown in Figure 3, both liposomes displayed the formation of unilamellar vesicles measuring 80-150 nm in diameter. It is notable that the liposomes interact with each other in the case of Na_2BSH-encapsulating liposomes, whereas the liposomes disperse in solution without interacting with each other in the case of spd-BSH-encapsulating liposomes.

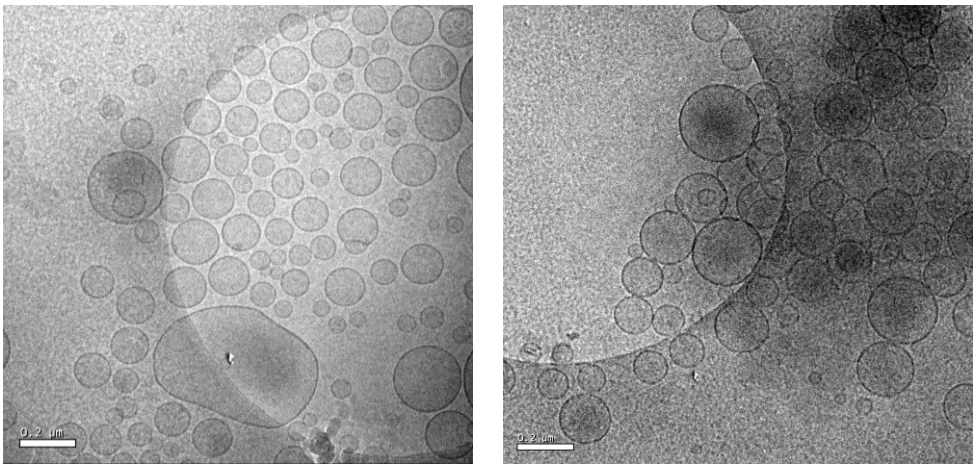

Figure 3. TEM images of spd-BSH-encapsulating liposomes (left) and Na_2BSH-encapsulating liposomes (right). Scale bar represents 200 nm.

2.2.6. Boron accumulation of spd-BSH-encapsulating liposome in colon 26 cells

The accumulation of the BSH cluster, BPA, Na_2BSH and spd-BSH encapsulating liposome in the mouse colorectal carcinoma cell line, colon 26, was examined. Colon 26 cells were incubated with 100 μM at 37°C for 1 h and then digested with perchloric acid/hydrogen peroxide (2/1 volume ratio) at 70°C for 6 h. Boron concentration in the resulting clear solution was measured by ICP-AES. As shown in Figure 4, a boron accumulation in colon 26 cells (1.0×10^6 cells) treated with spd-BSH-liposomes was twice of that of BSH liposomes, although a boron accumulation in the cancer cells by BSH liposomes similar to that of BSH(Na_2BSH) solution. The results indicate a boron accumulation in colon 26 cancer cells depend on B/P ratio as a boron concentration in a liposome.

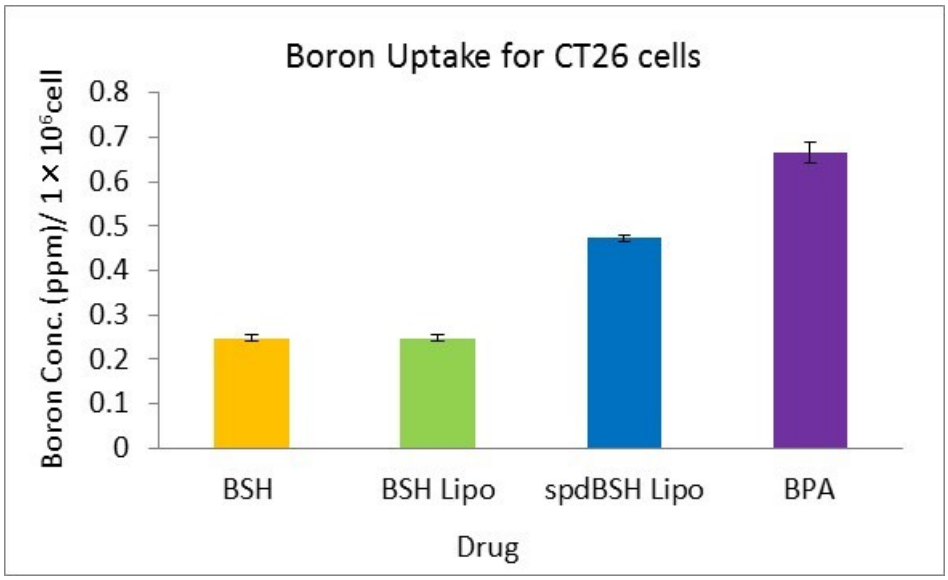

Figure 4. Boron Uptake in colon 26 cells (1.0×10^6 cells) incubated with each BSH (Orange), BSH liposomes (Green), spd-BSH (Blue) liposomes and BPA (purple). Data of triplicate experiments are expressed as means ±standard deviation.

2.2.7. Boron distribution in tumor-bearing mice injected with spd closo-*dodecaborate encapsulating liposomes*

Colon 26 tumor bearing mice were injected with spd-*closo*-dodecaborate-encapsulating liposomes at doses of 15, 30, and 100 mg [B]/kg body weight via the tail veins (five mice in each group). Na_2BSH- and $Na_2[B_{12}H_{11}NH_3]$-encapsulating liposomes at the dose of 30 mg [B]/kg were used as controls. At 24, 36, and 48 h after injection, the mice were lightly anesthetized, bled via the retro-orbital sinus, killed by cervical dislocation, and dissected. Both distribution and tumor accumulation of boron were determined by ICP-AES. Figure 5-A(a) shows the time courses of boron blood clearance after injection of BSH-encapsulating liposomes. Blood boron concentrations of 460.7, 104.0, and 33.2 ppm were detected 24 h after injection of spd-BSH-encapsulating liposomes (100, 30, and 15 mg [B]/kg), respectively. Blood boron concentration in mice injected with 100 mg [B]/kg of spd-BSH-encapsulating liposomes did not decrease notably during the 48-h period, whereas those in mice injected with 30 and 15 mg [B]/kg of spd-BSH-encapsulating liposomes gradually decreased in a time-dependent manner. Figures 5-A(b-d) show the time courses of boron concentrations in liver, kidney, and spleen, respectively. Time-dependent boron accumulation was observed in liver; boron concentrations of 528.47, 144.17, and 74.41 ppm were detected 48 h after the injection of 100, 30, and 15 mg [B]/kg of spd-BSH-encapsulating liposomes, respectively. In contrast, maximum boron accumulation in tumor was observed 36 h after injection; boron concentrations reached 202.7 and 82.4 ppm at doses of 100 and 30 mg [B]/kg, respectively. Even at the low boron dose of 15 mg [B]/kg, tumor boron concentration was 34.0 ppm and tumor/blood ratio was approximately 2 at 36 h after injection (Figure 4e). Since the required tumor boron concentration for BNCT is 30 ppm, these tumor boron concentrations are considered sufficient for BNCT. We also demonstrated the boron distribution of Na_2BSH-encapsulating liposomes in tumor-bearing mice for comparison. Although blood and liver boron concentrations after injection of Na_2BSH-encapsulating liposomes at the dose of 30 mg [B]/kg were similar to those after injection of spd-BSH-encapsulating liposomes

at the dose of 30 mg [B]/kg, kidney and spleen boron concentrations after injection of Na_2BSH-encapsulating liposomes were lower than those after injection of spd-BSH-encapsulating liposomes until 48 h. Tumor boron concentration at 36 h after injecting Na_2BSH-encapsulating liposomes was 31.9 ppm. However, the clearance rate of Na_2BSH-encapsulating liposomes was lower than that of spd-BSH-encapsulating liposomes (Figure 5-A(e)). A similar tendency was observed in spd-$[B_{12}H_{11}NH_3]$-encapsulating liposomes (Figure 5-B). Blood, kidney, and spleen boron concentrations gradually decreased after injecting spd-$[B_{12}H_{11}NH_3]$-encapsulating liposomes (Figures 4-B(a, 5c, and 5d)). Time-dependent boron accumulation was observed in liver at doses of 100 and 30 mg [B]/kg (Figure 5-B(b)). Maximum tumor boron accumulation was observed at 36 h after injection; tumor boron concentrations were 242.2, 88.7, and 35.4 ppm at doses of 100, 30, and 15 mg [B]/kg, respectively. Interestingly, significant tumor boron accumulation was also observed in the case of $Na[B_{12}H_{11}NH_3]$-encapsulating liposomes; tumor boron concentration was 25.4 ppm at the dose of 15 mg [B]/kg. Needless to say, acute toxicity was not observed even at such high doses as 50 and 100 mg [B]/kg.

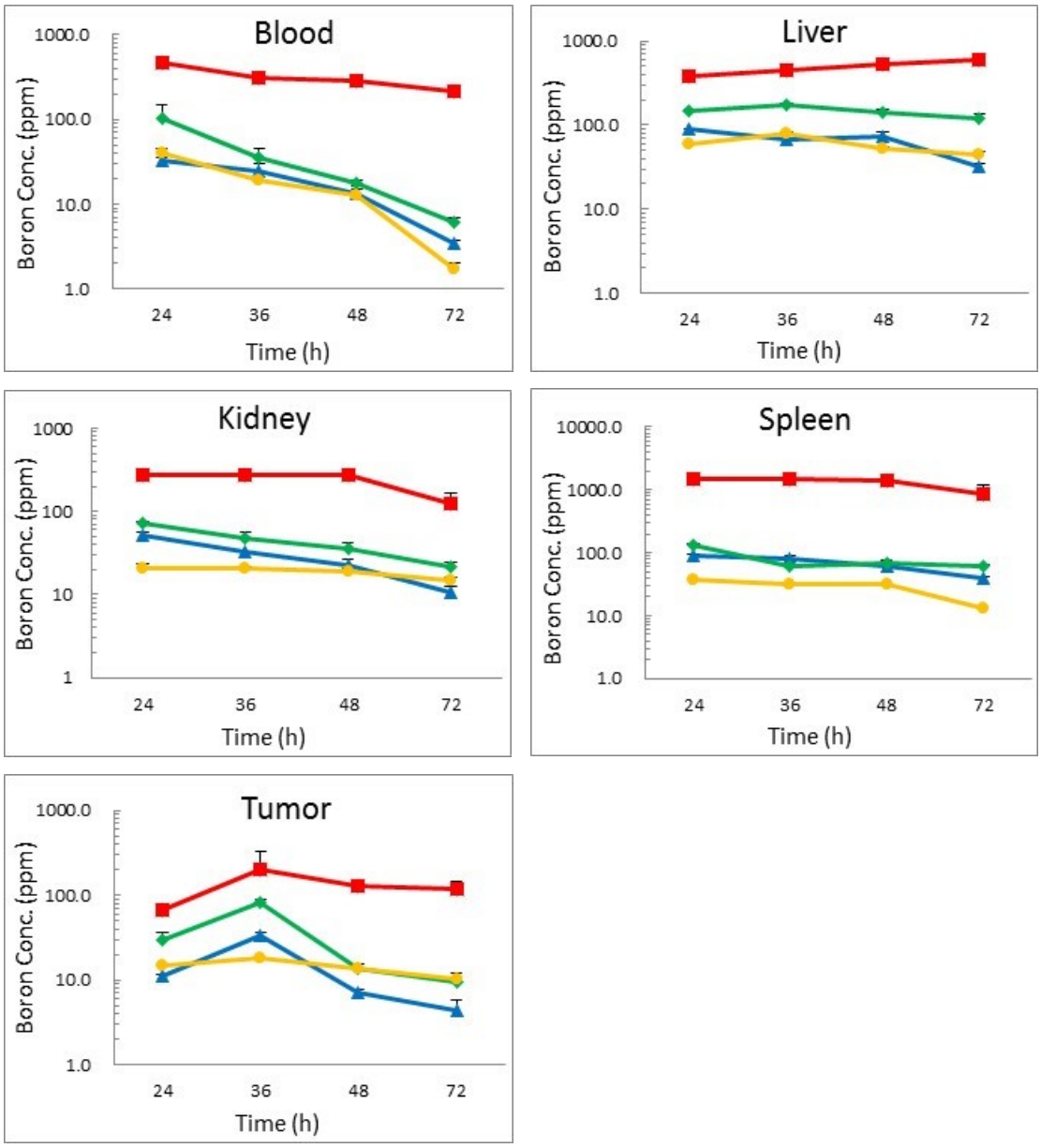

Figure 5-A. Time courses of distribution of spd-BSH- and Na_2BSH-encapsulating liposomes (▲Blue, spd-BSH: 15 mg[B]/kg; ◆Green, spd-BSH: 30 mg[B]/kg; ■Red, spd-BSH: 100 mg[B]/kg; ●Orange, Na_2BSH: 15 mg[B]/kg). Each liposome was injected into tumor-bearing mice (Balb/c, female, six weeks old, 14-20 g) via the tail vein.

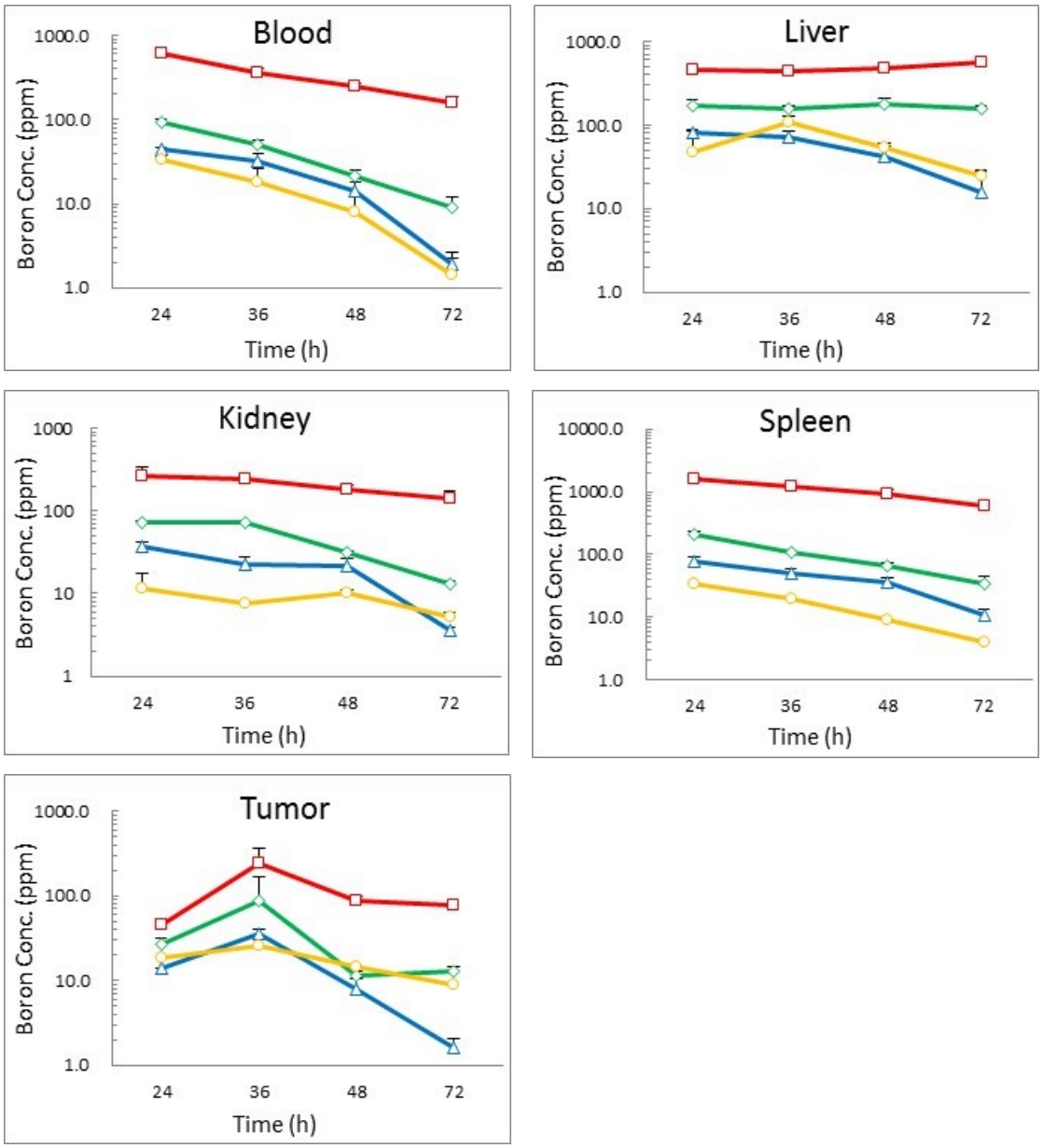

Figure 5-B. Time courses of distribution of spd-[$B_{12}H_{11}NH_3$]- and Na[$B_{12}H_{11}NH_3$]-encapsulating liposomes (△ Blue, spd-[$B_{12}H_{11}NH_3$]: 15 mg[B]/kg; ◇ Green, spd-[$B_{12}H_{11}NH_3$]: 30 mg[B]/kg; □ Red, spd-[$B_{12}H_{11}NH_3$]: 100 mg[B]/kg; ○ Orange, Na[$B_{12}H_{11}NH_3$]: 15 mg[B]/kg). Each liposome was injected into tumor-bearing mice (Balb/c, female, six weeks old, 14-20 g) via the tail vein.

2.2.8. BNCT for tumor-bearing mice injected with liposomes containing spd closo-*dodecaborates*

The antitumor effect of liposomes containing spd *closo*-dodecaborates in colon 26 tumor bearing mice exposed to thermal neutron irradiation was examined at the Kyoto University Reactor (KUR). Thermal neutron irradiation of the tumor-transplanted left thighs of mice was carried out 36 h after injection while shielding mouse bodies with an acrylic mouse holder (five mice in each group). The tumor growth curves of mice injected with spd-[^{10}BSH]- and Na_2[^{10}BSH]-encapsulating liposomes exposed to thermal neutron irradiation are shown in Figures 6A. Figure 6B shows the tumor growth curves of mice injected with spd-[$^{10}B_{12}H_{11}NH_3$]- and Na[$^{10}B_{12}H_{11}NH_3$]-encapsulating liposomes and exposed to thermal neutron irradiation. "Hot control (-○-)" and "Cold control (-✳-)" represent tumor volumes of mice injected with saline with and without thermal neutron irradiation, respectively. Significant inhibition of tumor growth was observed in mice treated with spd-[^{10}BSH]- and spd-[$^{10}B_{12}H_{11}NH_3$]-encapsulating liposomes at doses of 15, 30, and 100 mg [^{10}B]/kg and exposed thermal neutron irradiation, and the tumor disappeared within three weeks even the dose of 15 mg [^{10}B]/kg. Liposomes encapsulated with Na_2[^{10}BSH] and Na[$^{10}B_{12}H_{11}NH_3$] also showed inhibition of the tumor growth at the dose of 30 mg [^{10}B]/kg, however, the regrowth of the tumor was observed four weeks after thermal neutron irradiation. Tumor growth was suppressed in mice treated with Na_2[^{10}BSH] solution (100 mg [^{10}B]/kg) at least after thermal neutron irradiation. However, the tumor started to grow thereafter (Figure 6A). In contrast, tumor growth was not suppressed in mice treated with Na[$^{10}B_{12}H_{11}NH_3$] solution (100 mg [^{10}B]/kg) even thermal neutron irradiation (Figure 6B). In the case of lower neutron fluxes (0.48-0.96 × 10^{12} neutrons/cm^2), where the mice were irradiated for 12 min, the tumor growth was significantly suppressed only at the dose of 30 mg [^{10}B]/kg of liposomes encapsulated with spd-[^{10}BSH].

Figure 7 shows the survival curve of tumor-bearing mice after thermal neutron irradiation. The mice was irradiaed 36 h after injection of liposomes containing spd-[^{10}BSH] and spd-

[$^{10}B_{12}H_{11}NH_3$] at doses of 15 and 30 mg[^{10}B]/kg. All untreated mice without thermal neutron irradiation died in two weeks. Thermal neutron irradiation enhanced mouse survival and all mice exposed to theirmal neutron irradiation died within 78 days. Prolonged survival was observed in mice injected with spd-[^{10}BSH]- and spd-[$^{10}B_{12}H_{11}NH_3$]-encapsulating liposomes; 72% of the mice that received the dose of 15 mg [^{10}B]/kg survived up to 100 days after the thermal neutron irradiation. Furthermore, remarkable antitumor effect was observed in the mice injected with spd-[^{10}BSH]-encapsulating liposomes at the dose of 30 mg [^{10}B]/kg; 100% of the mice survived up to 100 days after the thermal neutron irradiation.

(A) $Na_2[^{10}BSH]$ and spd-$[^{10}BSH]$ encapsulationg liposomes

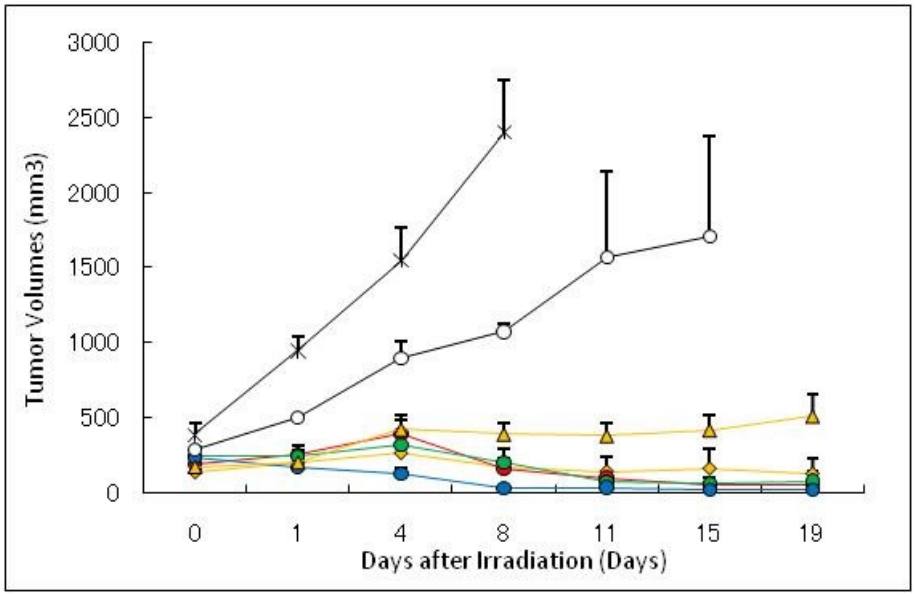

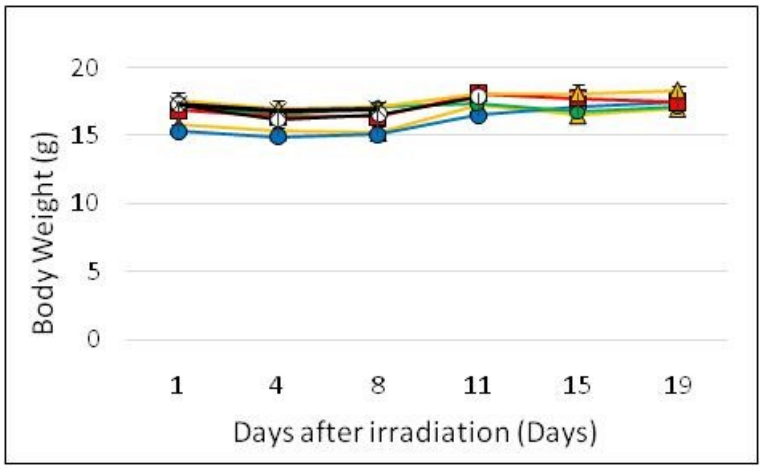

Figure 6-A. Tumor volumes in mice (Balb/c, female, six weeks old, 14-20 g) bearing colon 26 solid tumor, exposed to thermal neutron irradiation (hot) for 50 min (1.3-2.2 × 10^{12} neutrons/cm^2) or not exposed to thermal neutron irradiation (cold). (A) Irradiation was performed 36 h after injection of liposomes containing spd-$[^{10}BSH]$ (●Blue, 15; ● Green, 30; ●Red, 100 mg $[^{10}B]$/kg) and $Na_2[^{10}BSH]$ (◆Orange, 30 mg $[^{10}B]$/kg), or 1 h after injection of $Na_2[^{10}BSH]$ solution (▲Orange, 100 mg $[^{10}B]$/kg). ○, hot control; ✳, cold control.

(B) Na[$^{10}B_{12}H_{11}NH_3$] and spd-[$^{10}B_{12}H_{11}NH_3$] encapsulating liposomes

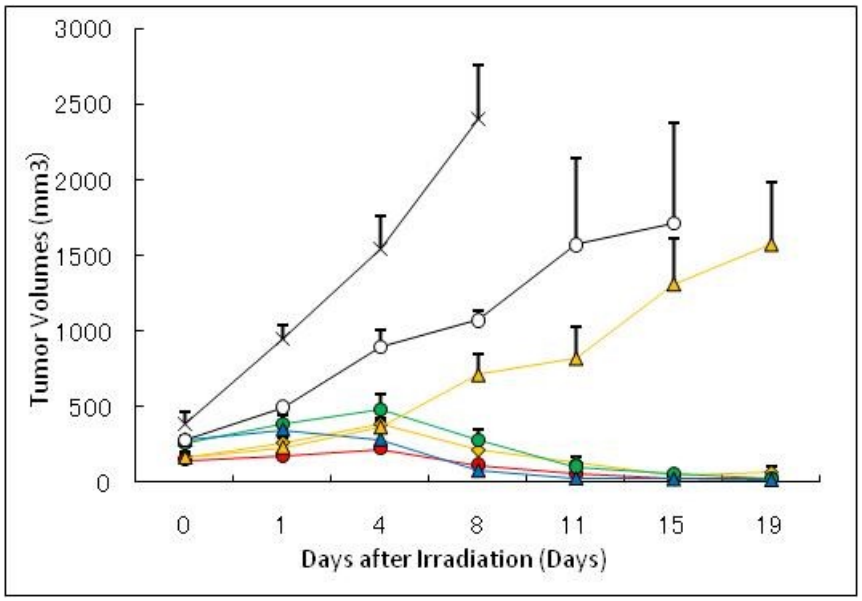

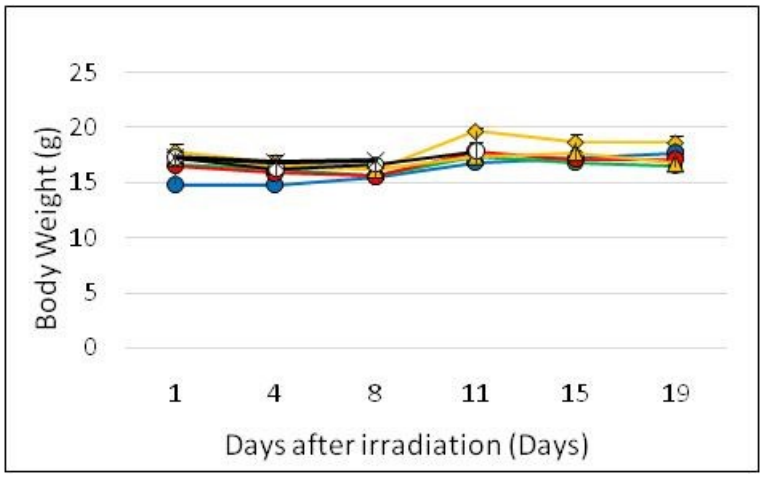

Figure 6-B. Tumor volumes in mice (Balb/c, female, six weeks old, 14-20 g) bearing colon 26 solid tumor, exposed to thermal neutron irradiation (hot) for 50 min (1.3-2.2 × 10^{12} neutrons/cm^2) or not exposed to thermal neutron irradiation (cold). (B) Irradiation was performed 36 h after injection of liposomes containing spd-[$^{10}B_{12}H_{11}NH_3$] (●Blue, 15; ●Green, 30; ●Red,100 mg [^{10}B]/kg) and Na[$^{10}B_{12}H_{11}NH_3$] (◆Orange, 30 mg [^{10}B]/kg), or 1 h after injection of Na[$^{10}B_{12}H_{11}NH_3$] solution (▲Orange, 100 mg [^{10}B]/kg). ○, hot control; ✳, cold control. Data are expressed as means ± sem (n = 7).

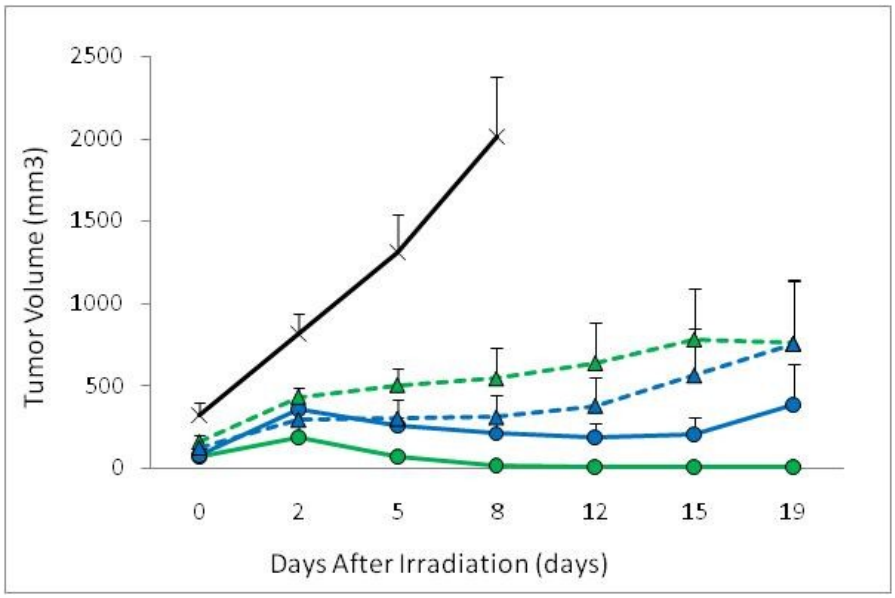

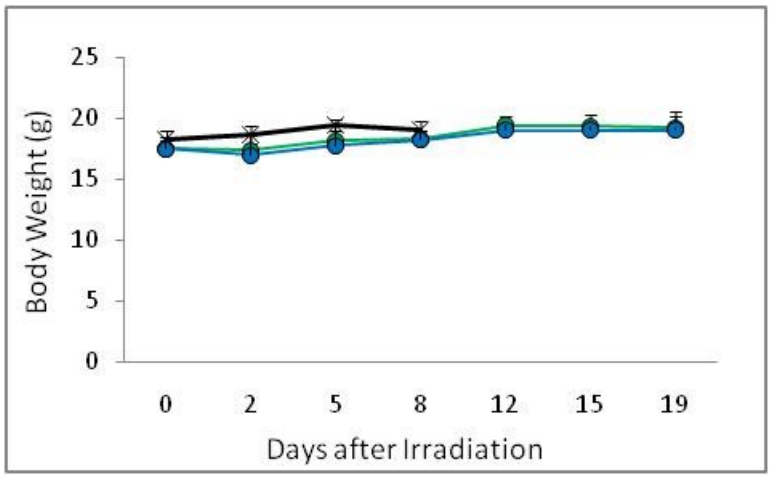

Figure 6-C. Tumor volumes in mice (Balb/c, female, six weeks old, 14-20 g) bearing colon 26 solid tumor, exposed to thermal neutron irradiation (hot) for 12-24 min (0.48-0.96 × 10^{12} neutrons/cm^2) or not exposed to thermal neutron irradiation (cold). (C) Irradiation was performed 36 h after injection of liposomes containing spd-[^{10}BSH] (● Blue, 15; ●Green, 30 [^{10}B]/kg : 0.96 × 10^{12} neutrons/cm^2; ▲Blue, 15; ▲Green, 30 [^{10}B]/kg : 0.48 × 10^{12} neutrons/cm^2;). ✳, cold control.

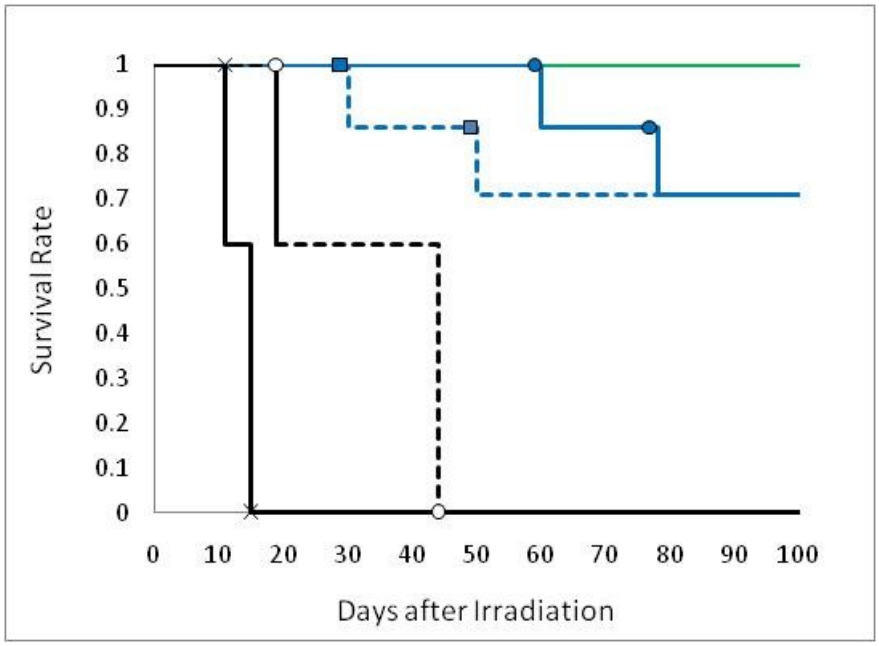

Figure 7. Survival curve of tumor-bearing mice after thermal neutron irradiation. The irradiation was performed 36 h after injection of *closo*-dodecaborates (−Green, spd-BSH: 30 mg[B]/kg; ● Blue, spd-BSH: 15 mg[^{10}B]/kg; ■ Blue, spd-$^{10}B_{12}H_{11}NH_3$: 15 mg[^{10}B]/kg) for 50 min (1.3-2.2 × 10^{12} neutrons/cm^2). ✳, Cold control; ○White, Hot control.

2.3. Discussion

Liposomes are one of the most attractive boron delivery vehicles because they can encapsulate a large number of ^{10}B atoms and transport them to tumor even though the boron compounds have low affinity to the tumor. The preparation of high boron content liposomes, however, is hampered by osmotic pressure limitations. To overcome this problem, we have developed various boron cluster lipids for the embedment of boron atoms into the liposomal membrane. [35-38] We have developed Na_2BSH-encapsulating 10% DSBL liposomes that have a B/P ratio of 2.6 and display excellent boron delivery to tumor. The total dose of Na_2BSH-encapsulating 10% DSBL liposomes could be reduced to less than one-fifth of that of BSH-encapsulating liposomes without lowering the efficacy of BNCT. [30] In the current study, we focused on three *closo*-dodecaborates, $Na[B_{12}H_{11}NH_3]$, $Na_2[B_{12}H_{11}OH]$, and $Na_2[B_{12}H_{12}]$, in addition to Na_2BSH, as the boron compounds to be encapsulated in the internal aqueous core of liposomes. As shown in Table 1, the cytotoxicity of those three *closo*-dodecaborates is lower than that of Na_2BSH (5.1~32.9 mM *vs*. 2.1 mM). Among the *closo*-dodecaborates, $Na[B_{12}H_{11}NH_3]$ is the most highly encapsulated in DSPC liposomes; final boron concentration of the liposome solution was 4,072 ppm and B/P ratio was 2.2 in the 125 mM *closo*-dodecaborate solution (entry 2 in Table 2). In the case of $Na[B_{12}H_{11}NH_3]$, an ammonium ion group served as one of the two counter cations of the *closo*-dodecaborate dianion. We speculated that ammonium counter cations would affect the encapsulation of *closo*-dodecaborates in liposomes. Recently, Detlef and coworkers reported that Na_2BSH induces aggregation and membrane rupture, increasing wall thickness of the liposome and triggering the release of liposome contents. [39, 40] They suggested that the aggregation would be caused by the interaction of Na_2BSH with the phosphatidylcholine moiety of DSPC in the liposomes. We predicted that encapsulation as well as liposome yield would be increased if we could reduce this interaction in the preparation of *closo*-dodecaborate-encapsulating liposomes. Thus, we prepared various ammonium salts of BSH and examined their encapsulation into liposomes (entries 5-9 in Table 2). We found that spd

closo-dodecaborates were the most easily encapsulated (entries 7 and 9). Final boron concentrations of the spd-BSH- and spd-[$B_{12}H_{11}NH_3$]-encapsulating liposome solutions were 13,867 ppm and 13,790 ppm, respectively, and these high boron content liposome solutions enabled us to increase the injection dose to 100 mg [B]/kg while limiting the total volume of one injection to 200 μL/mouse. Indeed, the B/P ratios of spd-BSH- and spd-[$B_{12}H_{11}NH_3$]-encapsulating liposomes were approximately three times higher than those of Na_2BSH-encapsulating liposomes. It has been reported that doxorubicin could be efficiently loaded into liposomes with a transmembrane $(NH_4)_2HPO_4$ gradient and retained in the liposomes at physiological pH. [41] We surmised that osmotic pressure and/or viscosity of the solution of spd-*closo*-dodecaborates in the internal aqueous core of liposomes would affect the high B/P ratios. However, as shown in Table 3, the spermidinium cation neither decreased the osmotic pressure nor increased the viscosity of the solution of spd-*closo*-dodecaborates in the internal aqueous core of liposomes. Interestingly, Cryo-TEM images showed that liposomes interacted with each other in the case of Na_2BSH-encapsulating liposomes, whereas liposomes dispersed in solution without interacting with each other in the case of spd-BSH-encapsulating liposomes, indicating that the spd cation prevented the interaction of anionic *closo*-dodecaborates with the phosphatidylcholine moiety of DSPC in the liposomes (Figure 3). As a result, the aggregation observed in the Na_2BSH-encapsulating liposomes was diminished and liposome yield was dramatically increased (entry 7 in Table 2). The spd cation not only enhances encapsulation efficiency but also maintains the high boron content in liposomes (Figure 2). Spd-BSH-encapsulating liposome with a high boron concentration resulted in a high boron accumulation in tumor cells. The high boron content of the spd-*closo*-dodecaborate-encapsulating liposomes enabled us to inject doses of up to 100 mg [B]/kg into tumor-bearing mice (Figures 5-A,B). The liposomes showed excellent boron delivery to tumor: tumor boron concentrations reached 203 and 242 ppm 36 h after injection with 100 mg [B/]kg of spd-BSH- and spd-[$B_{12}H_{11}NH_3$]-encapsulating liposomes, respectively. Such high boron accumulations are probably due to the high blood boron concentrations (315 and 353 ppm 36 h after injection with 100 mg [B]/kg of spd-BSH-

and spd-[$B_{12}H_{11}NH_3$]-encapsulating liposomes, respectively). Whereas tumor boron concentrations of 34.0 and 35.4 ppm were noted 36 h after injecting 15 mg [B]/kg of spd-BSH- and spd-[$B_{12}H_{11}NH_3$]-encapsulating liposomes, tumor boron concentrations of 20.6 and 25.4 ppm were observed 36 h after injecting the same dose of the corresponding sodium salts of *closo*-dodecaborate (Na_2BSH and $Na[B_{12}H_{11}NH_3]$) encapsulating liposomes, revealing that the currently investigated high boron content liposomes show approximately 1.5 times higher accumulation in tumor than conventional liposomes containing sodium salts of *closo*-dodecaborates. We also observed the efficient antitumor effect of spd-[^{10}BSH]- and spd-[$^{10}B_{12}H_{11}NH_3$]-encapsulating liposomes in combination with thermal neutron irradiation in tumor-bearing mice even at the dose of 15 mg [^{10}B]/kg, and the complete suppression of tumor growth 19 days after BNCT, as shown in Figure 6. It should be noted that the injection of Na_2BSH solution also suppressed tumor growth, whereas the injection of Na[$^{10}B_{12}H_{11}NH_3$] solution had no effect on tumor growth. The difference is probably due to the functional groups of *closo*-dodecaborate: a mercapto (SH) group could form an S-S bond with cysteine residues in organs to trigger accumulation in cells,[42] whereas no such interaction would occur for an ammonium (NH_3^+) group. The survival curves indicated that 100% of mice injected with 30 mg [^{10}B]/kg of spd-BSH-encapsulating liposomes survived up to 100 days after the thermal neutron irradiation, whereas 72% of mice injected with 15 mg [^{10}B]/kg of spd-[^{10}BSH]- and spd-[$^{10}B_{12}H_{11}NH_3$]-encapsulating liposomes survived up to 100 days after the thermal neutron irradiation. B/P ratios reached 3.4 and 3.5 in the case of spd-[^{10}BSH]- and spd-[$^{10}B_{12}H_{11}NH_3$]-encapsulating liposomes, respectively, indicating that the total amount of DSPC liposomes necessary for injection could be reduced to approximately 112 and 109 mg/kg, respectively. Meanwhile, approximately 743 mg/kg of DSPC liposomes is necessary to administer a boron dose of 35 mg [^{10}B]/kg in the case of Na_2BSH-encapsulating liposomes that have a B/P ratio of 1.2. Therefore, the spd-[^{10}BSH]- and spd-[$^{10}B_{12}H_{11}NH_3$]-encapsulating liposomes enabled us to reduce the total amount of phospholipids to less than one-seventh of those used to prepare Na_2[^{10}BSH]-encapsulating liposomes.

2.4. Conclusion

Liposomal boron carriers are one of the most efficient strategies for the delivery of the required amount of boron atoms to tumor. We succeeded in the preparation of high boron content liposomes. The use of spd cation as an alternative counter cation of *closo*-dodecaborates was essential for the preparation of high boron content liposome solutions (up to approximately 14,000 ppm boron concentration) having high B/P ratios (up to 3.5). The spd cation prevented the interaction of anionic *closo*-dodecaborates with the phosphatidylcholine moiety of DSPC in the liposomes, thereby suppressing the release of liposome contents and increasing liposome yield. Significant antitumor effect was observed in mice that received a single injection. The tumor completely disappeared three weeks after thermal neutron irradiation ((1.5−1.8) x 10^{12} neutrons/cm^2) and was locally controlled for 100 days after the irradiation even at the dose of 15 mg [^{10}B]/kg. The results indicate that the total amount of phospholipids could be reduced to less than one-seventh of those used to prepare Na_2BSH-encapsulating liposomes. We believe that the spd-*closo*-dodecab orate- encapsulating liposomes are a promising candidate for clinical use in BNCT.

2.5. Materials and Methods

2.5.1. Chemicals

DSPC (MC-8080) and DSPE-PEG (SUNBRIGHT DSPE-020CN) were purchased from Nippon Oil and Fats (Tokyo, Japan). Cholesterol was purchased from Kanto Chemical (Tokyo, Japan). $(Et_3NH)_2[B_{12}H_{12}]$ and $Na_2[B_{12}H_{11}SH]$ (Na_2BSH) were purchased from Katchem Ltd. (Praha, Czech Republic). $Na_2[^{10}B_{12}H_{12}]$ and $Na_2[^{10}B_{12}H_{11}SH]$ ($Na_2{}^{10}BSH$) were kindly supplied by Stella Chemifa Co. (Osaka, Japan). *Closo*-dodecaborates, $Na[B_{12}H_{11}NH_3]$, $Na_2[B_{12}H_{11}OH]$, and $Na[^{10}B_{12}H_{11}NH_3]$ were synthesized from $(Et_3NH)_2[B_{12}H_{12}]$ and $Na_2[^{10}B_{12}H_{12}]$ according the literature procedures [31, 32] and transformed into their sodium forms by an ion-exchange resin (Amberlite IR-120). All other chemicals were of the highest grade commercially available. Spermidinium chloride solution was prepared from spermidine and aqueous 1N HCl solution (1:3 molar ratio).

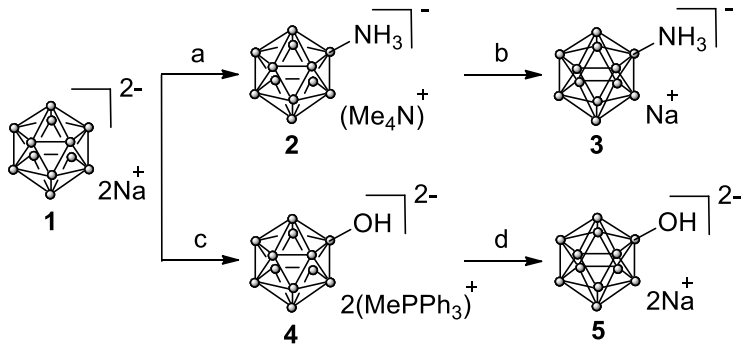

Scheme 1. Synthesis of $Na^{10}B_{12}H_{11}NH_3$ and $Na_2{}^{10}B_{12}H_{11}OH$.

Reagents and conditions: a. H_3NO_4S, Me_4NCl, H_2O, 80%. c. H_2SO_4, $CaCO_3$, $MePPh_3Br$, H_2O, 50%. b and d. Ion exchange with Amberlite IR120 (Na^+ form), **3**: 95%, **5**: 85%.

2.5.2. Cytotoxicity of sodium closo-dodecaborates toward cancer cells

Each sodium *closo*-dodecarborate (Na_2BSH, $Na[B_{12}H_{11}NH_3]$, $Na_2[B_{12}H_{11}OH]$ and $Na_2[B_{12}H_{12}]$) was dissolved in 1 mL of Phosphate buffered saline (PBS), and the solution was diluted with RPM1640 (1% penicillin and streptomycin, 10% fetal bovine serum (FBS). In 96 well plates, mouse colon 26 cells (5×10^3 cells/well) were cultured with the medium containing *closo*-dodecaborates at each concentration (0.1, 0.3, 1, 3, 10 and 30 mM) and incubated for 72 h at 37°C in a CO_2 incubator. Then the cell growth was determined by MTT Assay. Cell growth inhibition (GI_{50}) by concentration of each sodium *closo*-dodecarborate was determined from semi-logarithmic dose-response plots, and results represent the mean ± standard deviation (SD) of triplicate experiments.

2.5.3. Preparation of liposomes encapsulated with various ammonium salts of closo-dodecaborates

An aqueous solution of various ammonium chloride salts (1,4-diaminobutane, spermidine, and spermine) of *closo*-dodecaborates were prepared by adding sodium *closo*-dodecaborates to a mixture of each amine and aqueous 1N HCl solution (1:2, 1:3, 1:4 molar ratio, respectively PH=6-8). These ammonium *closo*-dodecaborates encapsulating liposome were prepared from DSPC, cholesterol and DSPE-PEG (1:1:0.11, molar ratio) by the reverse-phase evaporation (REV) method.[33] A mixture of DSPC (158 mg), cholesterol (77.3 mg), and DSPE-PEG-20CN (63.8 mg) were dissolved in 5 mL of a chloroform/ diisopropylether mixture (1 : 1, v/v) in a 50 mL round-bottom flask. An ammonium cation forms solution (1,4-diaminobutane, spermidine, and spermine) of *closo*-dodecaborates (125 mM, 5 mL) was added to the mixture to form a w/o emulsion. The emulsion was sonicated for 3 min, and then, the organic solvent was removed under vacuum in a rotary evaporator at 55 °C to obtain a suspending liposome solution. The liposomes obtained were subjected to extrusion 10 times through a polycarbonate

membrane of 100 nm pore size (Whatman, 110605, FILTER, 0.1 UM, 25 MM, Gentaur Molecular Products, Belgium), using an extruder device (LIPEX^{TM} Extruder, Northern Lipids, Canada). Purification was accomplished by ultracentrifuging at 200,000 g for 60 min at 4°C (himac cp 80 wx, Hitachi Koki, Japan), and the pellets obtained were resuspended in saline. Particle size and zeta potential of these liposomes were measured with an electrophoretic light scattering spectrophotometer (Nano-ZS, Sysmex, Japan). B/P (boron concentration / phosphorus concentration) ratio was calculated from data obtained by the simultaneous measurement of boron and phosphorus concentrations by inductively coupled plasma atomic emission spectroscopy (ICP-AES, HORIBA, Japan).

2.5.4. Effect of spermidinium cations on the formation of closo-dodecaborates encapsulating liposomes

The osmotic pressure of $(spd)_x$-BSH solutions (Na_2BSH: spermidine: HCl molar ratios = 1: X: 3X; X = 0.1, 0.5, 1, 2, and 10) was measured with an osmometer (Advanced Model 3250 Single-Sample Osmometer, Advanced Instruments, Inc.). The viscosity of spd-[B12H12] solution at various concentrations was measured by the viscometer (DV-1 + Viscometer, Brookfield, USA). Yields and B/P ratios of liposomes prepared from Na_2BSH, spermidine, and HCl (Na_2BSH: spermidine: HCl = 1: X: 3X; X = 0.5, 1.0, 1.5, and 2.0) were calculated from data obtained by the simultaneous measurement of boron and phosphorus concentrations by ICP-AES.

2.5.5. Leakage of encapsulated closo-dodecaborates from liposomes in saline

Spd-BSH- and spd-[$B_{12}H_{11}NH_3$]-encapsulating PEG-liposomes were prepared from DSPC, cholesterol and DSPE-PEG (1:1:0.11, molar ratio) in 1 : 1 and 2 : 1 mixtures of the corresponding sodium *closo*-dodecaborates (125 mM) and spermidinium hydrochloride in solusion. A pellet of the liposomes obtained after ultracentrifugation was resuspended in saline and the resulting liposome solutions were allowed to stand for one day at 25 °C. The B/P ratios of the liposomes were calculated from data obtained by measurement of boron and phosphorus concentrations by ICP-AES after ultracentrifugation at 200,000 x g for 60 min at 4 °C. The resulting liposome solutions were left to stand for another six days (seven days after preparation) at 25 °C and B/P ratios were calculated in a similar manner. This analysis was repeated 14 days after the preparation of liposomes.

2.5.6. Transmission electron microscopy analysis

Vitrified specimens were prepared by placing 3 μL of the studied sample suspension on a 400 mesh copper grid with a holey carbon support. Each sample was blotted to a thin film and immediately plunged into liquid ethane in the Leica CPC cryoworkstation. The grids were viewed on a JEOL 2011 transmission electron microscope operating at an accelerating voltage of 200 kV. The microscope was equipped with a Gatan cryoholder and the samples were maintained at -177ºC during imaging. Electron micrographs were recorded with the Digital Micrograph software package under low electron dose conditions, to minimize electron bean radiation. Images were recorded on a Gatan 794 MSC 600HP cooled charge-coupled device (CCD) camera.

2.5.7. Boron accumulation in colon 26 cells treated with liposomes encapsulated spd-closo-dodecarborate

The mouse colon 26 were cultured at 37ºC under 5% CO_2 atmosphere in RPMI 1640 medium supplemented with RPM1640 (1% penicillin and streptomycin, 10% fetal bovine serum (FBS). For subsequent experiments, the cells were seeded at a density of 1×10^5 cells in a 60 mm diameter dish (Greiner) and incubated at 37 °C for 24 h. Three dishes were used for cell counting (1.6×10^6 cells/dish). The cells in other dishes were incubated at 37°C in the presence of 100 μM of BSH cluster, BPA, Na_2BSH and spd-BSH-encapsulating liposomes for another 1 h and then washed three times with PBS. The cells were digested with 2 mL of perchloric acid/hydrogen peroxide at 70°C for 1 h and and then the digested samples were diluted with distilled water. After filtering through a hydrophobic filter (0.5 UM, 13JP050AN, ADVANTEC, Japan), the boron concentration was measured by ICP-AES.

2.5.8. Boron distribution of liposomes encapsulated spd-closo-dodecarborate in tumor-bearing mice

Tumor-bearing mice (Balb/c mice, female, 5-6 weeks old, 16-20 g, Sankyo Labo Service, Japan) were prepared by transplanting a suspension (1.0×10^6 cells / mouse) of colon 26 cells into subcutaneously (s.c.) of the right thigh. The mice were kept on a regular chow diet and water and maintained under 12 h light / dark cycle in an ambient atmosphere. Biodistribution experiments were performed when the tumor on mouse diameter grew 7 to 9 mm. The mice were injected via the tail vein at a dose of 15, 30, 100 mg [^{10}B]/kg (1,500, 3,000, 10,000 ppm ^{10}B concentration; 200 μL of spd-*closo*-dodecarborate encapsulating liposomes solution) and 15 mg [^{10}B]/kg (1,500 ppm ^{10}B concentration; 200 μL of sodium *closo*-dodecarborate encapsulating liposome solution). At selected time intervals (24, 36, 48, and 72 h) after administration, the mice were

lightly anesthetized and blood samples were collected from the retro-orbital sinus. The mice were then sacrificed by cervical dislocation and dissected. Liver, kidney, spleen, and tumor were excised, washed with 0.9% NaCl solution, and weighed. The excised organs were digested with 1 mL of conc. HNO_3 (ultratrace analysis grade, Wako, Japan) at 90°C for 1 h, and then the digested samples were diluted with distilled water. After filtering through a hydrophobic filter (0.5 UM, 13JP050AN, ADVANTEC, Japan), boron concentration of each organ was measured by ICP-AES.

2.5.9. BNCT effect on tumor-bearing mice treated with spd-closo-dodecarborate encapsulating liposomes.

Each spermidinium and sodium *closo*-dodecarborate encapsulating liposome was prepared from DSPC, cholesterol, and DSPE-PEG in a solution of ^{10}B-enriched *closo*-dodecaborates (spd-[^{10}BSH], spd-[$^{10}B_{12}H_{11}NH_3$], Na_2[^{10}BSH], or Na[$^{10}B_{12}H_{11}NH_3$]), by the REV method, and injected into colon 26 tumor-bearing mice (female, 5-6 weeks old, 16-20 g, Sankyo Labo Service, Japan) via the tail vein at a dose of 15, 30, 100 mg [^{10}B]/kg (1,500, 3,000, 10,000 ppm ^{10}B concentration; 200 μL of spd-*closo*-dodecarborate encapsulating liposomes solution) and 30 mg [^{10}B]/kg (3,000 ppm ^{10}B concentration; 200 μL of sodium *closo*-dodecarborate encapsulating liposome solution). The sodium *closo*-dodecarborate solutions at a dose of 100 mg [^{10}B]/kg (10,000 ppm of ^{10}B concentration; 200 μL) were used as a control experiments. The mice were anesthetized with isoflurane (Forane, Abbott, Japan) and placed in an acrylic mouse holder 36 h after i.v. injection based on biodistribution. The mice were irradiated in the KUR atomic reactor for 50 min at a rate of 1.3-2.2 × 10^{12} neutrons/cm^2. The BNCT effects were evaluated on the basis of the changes in tumor volume of the mice. Mortality was monitored daily and tumor volume was measured at intervals of a few days. To determine tumor volume, two perpendicular diameters of the tumor were measured with a slide

caliper and calculation was carried out using the formula $0.5(A \times B^2)$, where A and B are the longest and shortest dimensions of the tumor in millimeters, respectively. All protocols were approved by the Institutional Animal Care and Use Committee of Gakushuin University.

Statistical analysis.

The statistical significance of the results was analyzed using the Student's t test for unpaired observations and Dunnett's test for multiple comparisons.

2.6. Reference

[1] R.F. Barth, J.A. Coderre, M.G. Vicente, T.E. Blue, Boron neutron capture therapy of cancer: current status and future prospects, Clin. Cancer Res., 11 (2005) 3987-4002.

[2] T. Yamamoto, K. Nakai, A. Matsumura, Boron neutron capture therapy for glioblastoma, Cancer Lett., 262 (2008) 143-152.

[3] H. Hatanaka, A revised boron-neutron capture therapy for malignant brain tumors, J. Neurol., 209 (1975) 81-94.

[4] A.H. Soloway, W. Tjarks, B.A. Barnum, F.G. Rong, R.F. Barth, I.M. Codogni, J.G. Wilson, The Chemistry of Neutron Capture Therapy, Chem. Rev., 98 (1998) 1515-1562.

[5] A.H. Soloway, H. Hatanaka, M.A. Davis, Penetration of Brain and Brain Tumor. VII. Tumor-Binding Sulfhydryl Boron Compounds1,2, J. Med. Chem., 10 (1967) 714-717.

[6] Y. Nakagawa, H. Hatanaka, Boron neutron capture therapy: Clinical brain tumor studies, J. Neurooncol., 33 (1997) 105-115.

[7] T. Kageji, Y. Nakagawa, K. Kitamura, K. Matsumoto, H. Hatanaka, Pharmacokinetics and boron uptake of BSH (Na2B12H11SH) in patients with intracranial tumors, J. Neurooncol., 33 (1997) 117-130.

[8] Y. Mishima, C. Honda, M. Ichihashi, H. Obara, J. Hiratsuka, H. Fukuda, H. Karashima, T. Kobayashi, K. Kanda, K. Yoshino, TREATMENT OF MALIGNANT MELANOMA BY SINGLE THERMAL NEUTRON CAPTURE THERAPY WITH MELANOMA-SEEKING 10B-COMPOUND, The Lancet, 334 (1989) 388-389.

[9] Y. Mishima, M. Ichihashi, S. Hatta, C. Honda, K. Yamamura, T. Nakagawa, New thermal neutron capture therapy for malignant melanoma: melanogenesis-seeking 10B molecule-melanoma cell interaction from in vitro to first clinical trial, Pigment Cell Res., 2 (1989) 226-234.

[10] S.-I. Miyatake, Y. Tamura, S. Kawabata, K. Iida, T. Kuroiwa, K. Ono, Boron Neutron Capture Therapy for Malignant Tumors Related To Meningiomas, Neurosurgery, 61 (2007) 82-91

[11] I. Kato, K. Ono, Y. Sakurai, M. Ohmae, A. Maruhashi, Y. Imahori, M. Kirihata, M. Nakazawa, Y. Yura, Effectiveness of BNCT for recurrent head and neck malignancies, Appl. Radiat. Isot., 61 (2004) 1069-1073.

[12] T. Aihara, J. Hiratsuka, N. Morita, M. Uno, Y. Sakurai, A. Maruhashi, K. Ono, T. Harada, First clinical case of boron neutron capture therapy for head and neck malignancies using 18F-BPA PET, Head Neck, 28 (2006) 850-855.

[13] L. Kankaanranta, T. Seppälä, H. Koivunoro, K. Saarilahti, T. Atula, J. Collan, E. Salli, M. Kortesniemi, J. Uusi-Simola, A. Mäkitie, M. Seppänen, H. Minn, P. Kotiluoto, I. Auterinen, S. Savolainen, M. Kouri, H. Joensuu, Boron Neutron Capture Therapy in the Treatment of Locally Recurred Head and Neck Cancer, International Journal of Radiation Oncology*Biology*Physics, 69 (2007) 475-482.

[14] Y. Takahashi, Y. Imahori, K. Mineura, Prognostic and Therapeutic Indicator of Fluoroboronophenylalanine Positron Emission Tomography in Patients with Gliomas, Clin. Cancer Res., 9 (2003) 5888-5895.

[15] A. Wittig, W.A. Sauerwein, J.A. Coderre, Mechanisms of transport of p-borono-phenylalanine through the cell membrane in vitro, Radiat. Res., 153 (2000) 173-180.

[16] G.W. Kabalka, M.L. Yao, The synthesis and use of boronated amino acids for boron neutron capture therapy, Anticancer Agents Med. Chem., 6 (2006) 111-125.

[17] Y. Imahori, Y. Ohmori, R. Fujii, K. Matsumoto, S. Ueda, Rapid Incorporation of Carbon-11-labeled Diacylglycerol as a Probe of Signal Transduction in Glioma, Cancer Res., 55 (1995) 4225-4229.

[18] M. Suzuki, H. Tanaka, Y. Sakurai, G. Kashino, L. Yong, S. Masunaga, Y. Kinashi, T. Mitsumoto, S. Yajima, H. Tsutsui, T. Sato, A. Maruhashi, K. Ono, Impact of accelerator-based boron neutron capture therapy (AB-BNCT) on the treatment of

multiple liver tumors and malignant pleural mesothelioma, Radiother. Oncol., 92 (2009) 89-95.

[19] H. Tanaka, Y. Sakurai, M. Suzuki, T. Takata, S. Masunaga, Y. Kinashi, G. Kashino, Y. Liu, T. Mitsumoto, S. Yajima, H. Tsutsui, M. Takada, A. Maruhashi, K. Ono, Improvement of dose distribution in phantom by using epithermal neutron source based on the Be(p,n) reaction using a 30 MeV proton cyclotron accelerator, Appl. Radiat. Isot., 67 (2009) S258-261.

[20] Y. Matsumura, H. Maeda, A new concept for macromolecular therapeutics in cancer chemotherapy: mechanism of tumoritropic accumulation of proteins and the antitumor agent smancs, Cancer Res., 46 (1986) 6387-6392.

[21] H. Maeda, J. Wu, T. Sawa, Y. Matsumura, K. Hori, Tumor vascular permeability and the EPR effect in macromolecular therapeutics: a review, J. Control. Release, 65 (2000) 271-284.

[22] J. Folkman, Angiogenesis: an organizing principle for drug discovery?, Nature Reviews Drug Discovery, 6 (2007) 273-286.

[23] H. Nakamura, Chapter 10 - Liposomal Boron Delivery for Neutron Capture Therapy, in: D. Nejat (Ed.) Methods Enzymol., Academic Press, 2009, pp. 179-208.

[24] H. Nakamura, Boron lipid-based liposomal boron delivery system for neutron capture therapy: recent development and future perspective, Future Med. Chem., 5 (2013) 715-730.

[25] K. Maruyama, O. Ishida, S. Kasaoka, T. Takizawa, N. Utoguchi, A. Shinohara, M. Chiba, H. Kobayashi, M. Eriguchi, H. Yanagie, Intracellular targeting of sodium mercaptoundecahydrododecaborate (BSH) to solid tumors by transferrin-PEG liposomes, for boron neutron-capture therapy (BNCT), J. Control. Release, 98 (2004) 195-207.

[26] D.A. Feakes, K. Shelly, M.F. Hawthorne, Selective boron delivery to murine tumors by lipophilic species incorporated in the membranes of unilamellar liposomes, Proc. Natl. Acad. Sci. U. S. A., 92 (1995) 1367-1370.

[27] P.J. Kueffer, C.A. Maitz, A.A. Khan, S.A. Schuster, N.I. Shlyakhtina, S.S. Jalisatgi, J.D. Brockman, D.W. Nigg, M.F. Hawthorne, Boron neutron capture therapy demonstrated in mice bearing EMT6 tumors following selective delivery of boron by rationally designed liposomes, Proceedings of the National Academy of Sciences, 110 (2013) 6512-6517.

[28] J.-D. Lee, M. Ueno, Y. Miyajima, H. Nakamura, Synthesis of Boron Cluster Lipids: closo-Dodecaborate as an Alternative Hydrophilic Function of Boronated Liposomes for Neutron Capture Therapy, Org. Lett., 9 (2007) 323-326.

[29] M. Ueno, H.S. Ban, K. Nakai, R. Inomata, Y. Kaneda, A. Matsumura, H. Nakamura, Dodecaborate lipid liposomes as new vehicles for boron delivery system of neutron capture therapy, Biorg. Med. Chem., 18 (2010) 3059-3065.

[30] H. Koganei, M. Ueno, S. Tachikawa, L. Tasaki, H.S. Ban, M. Suzuki, K. Shiraishi, K. Kawano, M. Yokoyama, Y. Maitani, K. Ono, H. Nakamura, Development of High Boron Content Liposomes and Their Promising Antitumor Effect for Neutron Capture Therapy of Cancers, Bioconjug. Chem., 24 (2013) 124-132.

[31] W.R. Hertler, M.S. Raasch, Chemistry of Boranes. XIV. Amination of B10H10-2 and B12H12-2 with Hydroxylamine-O-sulfonic Acid, J. Am. Chem. Soc., 86 (1964) 3661-3668.

[32] T. Peymann, C.B. Knobler, M.F. Hawthorne, A Study of the Sequential Acid-Catalyzed Hydroxylation of Dodecahydro-closo-dodecaborate(2−), Inorg. Chem., 39 (2000) 1163-1170.

[33] F.J. Szoka, D. Papahadjopoulos, Procedure for preparation of liposomes with large internal aqueous space and high capture by reverse-phase evaporation, Proc. Natl. Acad. Sci. U. S. A., 75 (1978) 4194-4198.

[34] H. Hatanaka, Y. Nakagawa, Clinical results of long-surviving brain tumor patients who underwent boron neutron capture therapy, International Journal of Radiation Oncology Biology Physics, 28 (1994) 1061-1066.

[35] H. Nakamura, Y. Miyajima, T. Takei, S. Kasaoka, K. Maruyama, Synthesis and vesicle formation of a nido-carborane cluster lipid for boron neutron capture

therapy, Chem. Commun., (2004) 1910-1911.

[36] Y. Miyajima, H. Nakamura, Y. Kuwata, J.D. Lee, S. Masunaga, K. Ono, K. Maruyama, Transferrin-loaded nido-carborane liposomes: tumor-targeting boron delivery system for neutron capture therapy, Bioconjug. Chem., 17 (2006) 1314-1320.

[37] J.D. Lee, M. Ueno, Y. Miyajima, H. Nakamura, Synthesis of boron cluster lipids: closo-dodecaborate as an alternative hydrophilic function of boronated liposomes for neutron capture therapy, Org. Lett., 9 (2007) 323-326.

[38] M. Ueno, H.S. Ban, K. Nakai, R. Inomata, Y. Kaneda, A. Matsumura, H. Nakamura, Dodecaborate lipid liposomes as new vehicles for boron delivery system of neutron capture therapy, Bioorg. Med. Chem., 18 (2010) 3059-3065.

[39] D. Gabel, D. Awad, T. Schaffran, D. Radovan, D. Daraban, Luminita Damian, M. Winterhalter, G. Karlsson, K. Edwards, The Anionic Boron Cluster (B12H11SH)2- as a Means To Trigger Release of Liposome Contents, ChemMedChem, 2 (2007) 51-53.

[40] D. Awad, L. Damian, M. Winterhalter, G. Karlsson, K. Edwards, D. Gabel, Interaction of Na2B12H11SH with dimyristoyl phosphatidylcholine liposomes, Chem. Phys. Lipids, 157 (2009) 78-85.

[41] A. Fritze, F. Hens, A. Kimpfler, R. Schubert, R. Peschka-Süss, Remote loading of doxorubicin into liposomes driven by a transmembrane phosphate gradient, Biochimica et Biophysica Acta (BBA) - Biomembranes, 1758 (2006) 1633-1640.

[42] P.-P.P. Zhu Tang, M.P. Schweizer, K.M. Bradshaw, W.F. Bauer, 11B nuclear magnetic resonance studies of the interaction of borocaptate sodium with serum albumin, Biochem. Pharmacol., 49 (1995) 625-632

Synthesis of Protoporphyrin-Lipids (PL): Methods and Mechanism of Effective PDT with PL-Micelle & PL-Liposomes

3.1. Introduction

Photodynamic therapy (PDT) is an effective tumor treatment that uses a combination of photosensitizer (PS), oxygen, and proper weavelength light exciting PS. [1-4] Reactive oxygen species (ROS) generated from light to molecular oxygen by energy transfer (Type I reaction; single oxygen) and electron transfer (Type II reaction; superoxide, hydrogen peroxide and hydroxyl radicals) of photosensitizer induce significant oxidative damage of cellular biomolecules, leading to cell death in PDT. [5] Therefore, selective accumulation of PS in the target cells are important elements for successful application of PDT. Currently, Hematoporphyrin®, Photofrin® (QLT Photo Therapeutics Inc.), Visudyne® (Verteporfin^{TM}QLT Photo-Therapeutics Inc.), Levulan® (5-aminolevulinic acid, 5-ALA) have been approved as PDT drugs by the Food and Drug Administration in the US. [6] Hematoporphyrin (HpD) [7] is used for the treatment of cervical, endobronchial, esophageal, bladder, and gastric cancers. [2] Photofrin is used for the treatment of non-small-cell lung cancer (NSCL) and esophageal cancer. Visudyne (Verteporfin) is a second-generation photosensitizer that has a longer wavelength for its activation than Photofrin. [8] Visudyne is a liposomal formulation of Verteporfin and has been used for the treatment of age-related macular degeneration. [9] 5-ALA is a pro-drug that can be converted into PpIX in the biosynthetic pathway to allow a selective accumulation of PpIX in tumor after administration of 5-ALA. [10] However, in the adequate clinical treatment, high doses of 5-ALA is necessary in administration to be administered to reach therapeutic effect levels of PpIX. [11] So far, PpIX cannot be directly injected intravenously due to its low water solubility. Also, almost of clinically approved PDT drugs based on a porphyrin skeleton are hydrophobic and low water soluble. [12,13] Therefore, much attention has been focused on drug-delivery vehicles as nanoscale drug-delivery platforms such as liposomes. [14], dendrimers [15], and micelle [16,17] . Two types of strategy for liposomal delivery of photosensitizers have been mainly developed: (1) encapsulation of water-soluble photosensitizers in aqueous inner of liposomes (Figure 1A), and (2) accumulation of hydrophobic photosensitizers in

liposomal bilayer (Figure 1B). Our interest is the development of a water-soluble PpIX having amphiphilic property. Therefore, we focused on the vinyl and carboxylic acid groupss on PpIX and designed PpIX lipids having long alkyl chains and lithium carboxylates on PpIX, expecting their micelle formations in water. Recently, porphysomes that are liposome-like nanoparticles self-assembled by porphyrin lipids in a 100 nm-diameter, have been reported for biophotonic imaging and therapy. [18-19] In this chaper, I describe the synthesis of PpIX lipids and their micelle formations. I developed an alternative strategy for liposomal delivery of photosensitizers: post-insertion of PpIX-lipids in liposomal bilayer (Figure 1C). The advantage of PpIX-lipid post-inserted liposomes is able to prevent aggregation, which may interfere with PDT effect and decrease the fluorescence of the porphyrin dye. I describe the synthetic approach of PL-liposomes and their distribution and ROS function in the cells. The investigation would contribute to the fundamental understanding of PDT effects by porphyrin liposomes, which will facilitate the implementation of these nano photosensitizers for cancer therapy.

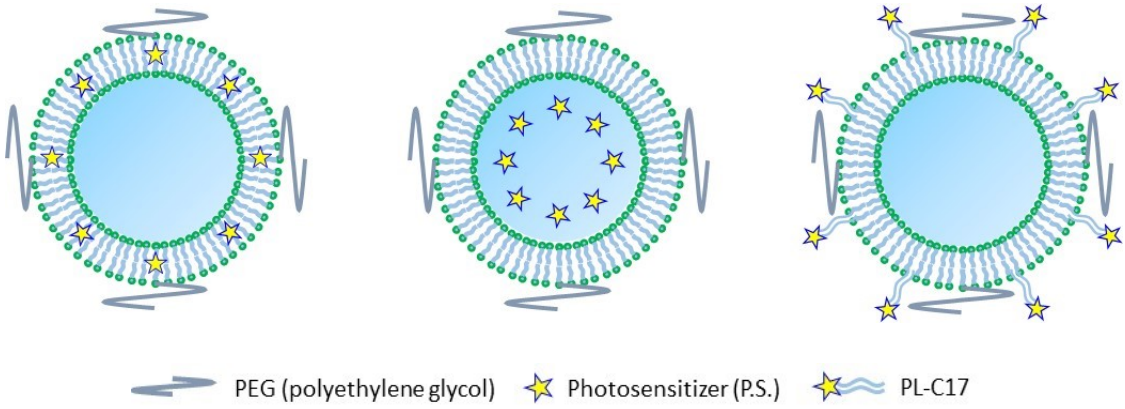

Figure 1. Photosensitizer liposome; (left) Encapsulation of water-soluble photosensitizers in the aqueous interior of liposomes. (center) Accumulation of hydrophobic photosensitizers in the liposomal bilayer. (right) Post-insertion of PpIX lipids into liposomal bilayer (the approach used in this study).

3.2. Results and Discussion

3.2.1. Synthesis of PpIX-lipids.

The synthetic route of PpIX-lipids is shown in Scheme 1. Acid esterification of protoporphyrin IX (PpIX; **1**) in the presence of H_2SO_4 in MeOH at -10 ^oC gave protoporphyrin IX dimethyl ester **2** in 95% yield. The vinyl groups of **2** were hydrobrominated with HBr/AcOH (25%) to yield the corresponding bis(α-methyl-β-bromo) protoporphyrin IX dimethyl ester **3**, which was then immediately treated with 1-tridecanol, 1-pentadecanol, and 1-heptadecanol in the presence of cesium carbonate (Cs_2CO_3) for 2 h at room temperature to give the corresponding ethers **4a-c** in 18-23% yields. Finally, hydrolysis of **4a-c** with LiOH•H_2Oin a mixed solvent system of THF/MeOH/H_2O (1:1:1) for 6 h afforded PpIX-lipids (**PL-C13**, **PL-C15**, and **PL-C17**) in high yields.

Scheme 1. Synthesis of PpIX lipids

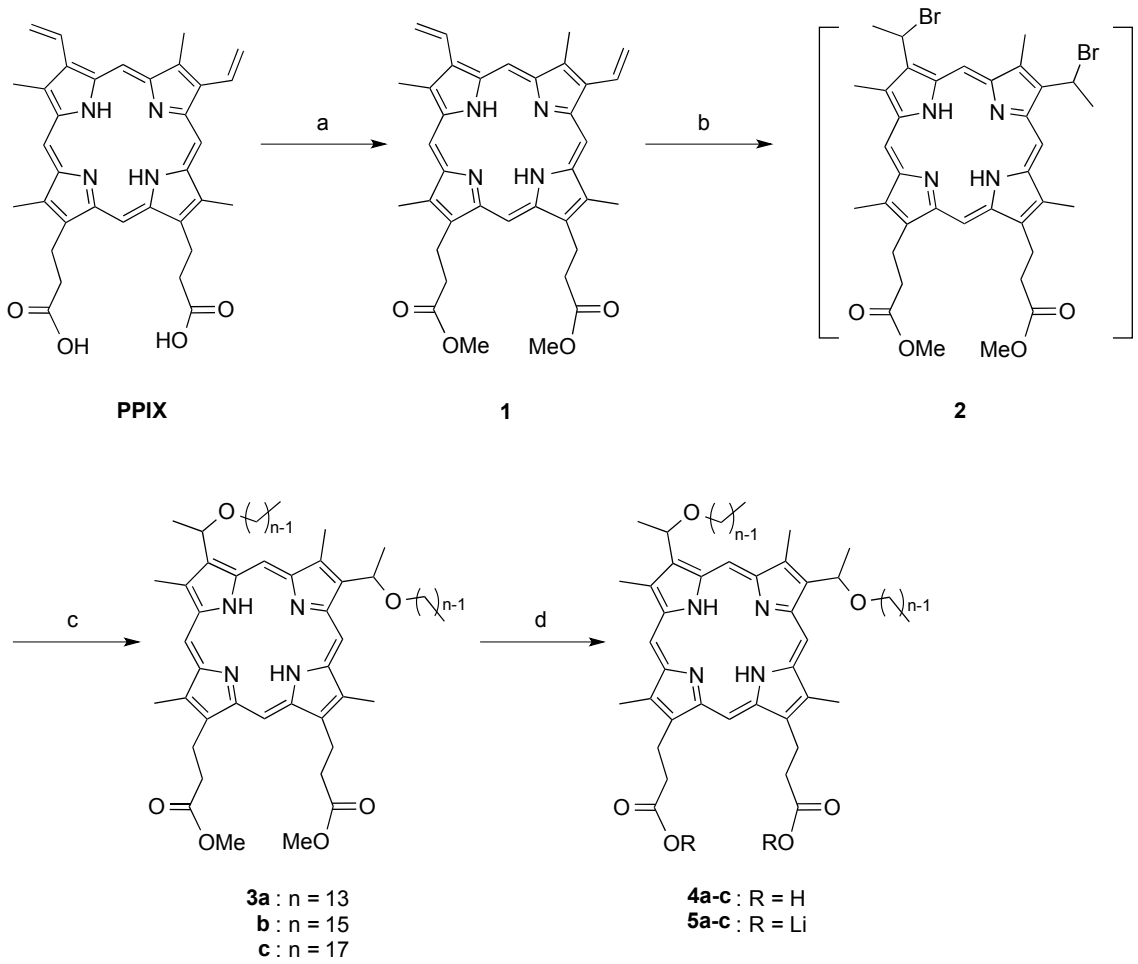

***Reagents and conditions*:** a. H_2SO_4, MeOH, -10 °C, 18 h, 95%; b.HBr, AcOH, r.t., 2h; c. ROH, CH_2Cl_2, K_2CO_3, r.t., 2h, **3a**; 23%, **3b**; 18%, **3c**; 21% in two steps; d. (i) LiOH, MeOH/H_2O/THF (1:1:1), r.t., 6h; (ii) HCl (1N), **4a**; 90%, **4b**; 90%, **4c**; 93%.

3.2.2. Characterization and cytotoxicity of PpIX lipid micelles

To an aqueous lithium hydroxide solution was added PpIX-lipids, such as PL-C13, PL-C15, or PL-C17, dissolved in THF and methanol solution, and the mixture was stirred until the hydrolysis was completed. THF was removed under the reduced pressure and the resulting lithium salts (**5a-c**) of PpIX-lipids were dissolved in water (1 mL) to form micelles. Particle size distributions, zeta potentials and cytotoxicity of these PpIX-lipid micelles are summarized in Table 1. PpIX-lipid micelles were distributed in the rage of 78.8-745.6 nm with average sizes of 585.3, 510.3, and 588.1 nm and peak sizes of 712.4, 615.1, and 615.1 nm for PL-C13, PL-C15, and PL-C17 micelles, respectively. These results indicate that PpIX-lipid micelles forms relatively large aggrigates in water. PpIX-lipids micelles exhibited similar average zeta potentials of -8.51 to -6.54mV, revealing that PpIX-lipid micelles are negatively charged due to two carboxylate moieties in their molecules. Cytotoxicity of PpIX-lipid micelles toward HeLa cells without light irradiation was indicated as a half maximal (50%) inhibitory concentration of cell growth. As shown in Table 1, PpIX-lipid micelles are relatively low toxic and their IC_{50} values toward HeLa cells are 379.9, 151.7, and 355.1 μM, respectively.

Table 1. Characterization of PpIX-Lipid Micelles[a]

PpIX lipid	Average size (nm)	Peak size (nm)	Zeta Potential(mV)	IC_{50}[b] (μM)
PL-C13	585.3 ± 7.4	712.4	-6.54 ± 11.8	379.9 ± 54.9
PL-C15	510.3 ± 12.8	615.1	-8.51 ± 18.9	151.7 ± 4.1
PL-C17	588.1 ± 15.8	615.1	-6.86 ± 12.0	355.1 ± 20.9

[a]Particle size (diameter)distributions and zeta potentials of PpIX-lipid micelles were measured by an electrophoretic light scattering spectrophotometer (Nano-ZS, Sysmex, Japan). [b]HeLa cells (5×10^3 cells per well of a 96-well plate) were incubated at 37°Cfor 72 h in RPMI-1640 medium (100 μL) containing various concentrations of the PpIX-lipid micelles. After the incubation, the cell viability was determined by the MTT assay. The drug concentration required to reduce cell viability by 50% (IC_{50}) was determined from semilogarithmic dose-responseplots.

3.2.3. Preparation and characterization of PL-C17 liposomes.

PL-C17 micelles were selected for preparation of PL-C17 liposomes by a post insertion method, because PL-C17 micelle showed low cytotoxicity and two long alkyl chain similar to DSPC having higher phase transition. PEG-liposomes were prepared from DSPC, Cholesterol and DSPE-PEG (1:1:0.11, molar ratio) by the reverse-phase evaporation (REV) method. The liposomes were purified by ultracentrifuging at 200,000 g for 60 min at 4 °C after through a polycarbonate membrane of 100 nm pore size. The PL-C17 micelle solution was added to the liposome solutionwith DSPC/PL-C17 molar ratios of 1:0.05-0.2 to generate PL-C17 liposomes. Figure 2A shows the liposome solution mixed with the PL-C17 micelles. After ultracentrifuging at 200,000 g for 60 min at 4 °C, the supernatant obtained was colorless as shown in Figure 2B, revealing that all PL-C17 lipids were inserted in the liposomes at the DSPC/PL-C17 molar ratio of 1:0.2. The particle size and zeta potential of PL-C17 liposomes were measured by the

electrophoretic light scattering spectrophotometer. As shown in Figure 2C, the size of liposomes increased with the molar ratio: the original liposome size was 113 nm whereas the sizes of PL-C17 liposomes with molar ratios of 1:0.05-0.2 were average diameters of 138.5 to 176.9 nm. These results indicate that the post insertion of PL-C17 lipids increases liposome sizes with increasing PL-C17 contents. PL-C17 liposomes with molar ratios of 1:0.05-0.2 showed similar zeta potentials of -32.6 to -45.8 mV, although the zeta potential of the original liposomes was -16.8 mV. A concentartion of PL-C17 post-inserted into PEG-liposome was determined by a standard curve of the concentration-dependent PL-C17 fluorescence intensity (Figure 4.).

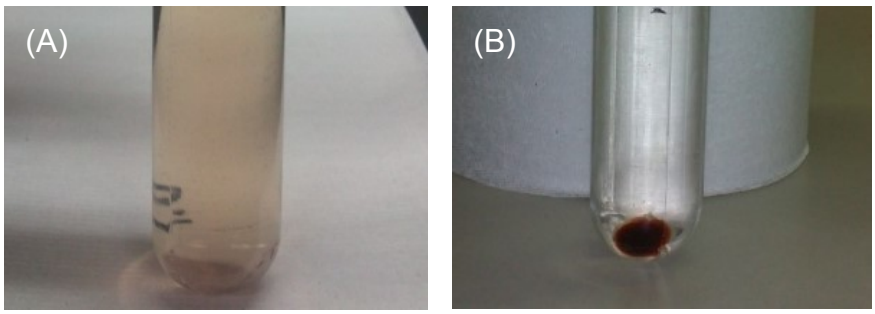

(C)

DSPC/PL-C17	Size (nm)	Zeta (mV)
1 : 0	113.5±0.9	-16.8 ± 18.1
1 : 0.05	138.5 ± 1.4	-32.6 ± 13.5
1 : 0.1	149.9±2.6	-46.0±10.9
1 : 0.2	176.9±1.3	-45.8±16.2

Figure 2. The liposome solutions mixed with the PL-C17 micelles before ultracentrifuging (A) and after ultracentrifuging (B). Sizes and zeta potentials of the liposomes in various ratios of DSPC/PL-C17 (C).

3.2.4. Absorbance of PpIX, PL-C17 micelles, and PL-C17 liposomes.

UV/V is absorbance of PpIX, PL-C17 micelles, and PL-C17 liposomes were measured over the 300–700 nm wavelength range. The UV/Vis spectra of PpIX, PL-C17 micelles, and PL-C17 liposomes in H_2O (10 μM) are shown in Figure 3. Each spectrum contains a high-energy Soretband (peak position=ca. 409 nm) and lower-energy Q bands (peak positions=ca. 512, 546, 584, 637 nm) arising from p–p* transitions, typical for the PpIX (**1**) framework. [20] Although a maximum absorbance peak of PpIX was observed at 409 nm, the maximum absorbance peaks of PL-C17 micelles and liposomes was lower and wider than that of PpIX probably due to the aggregation of PL-C17. [21]

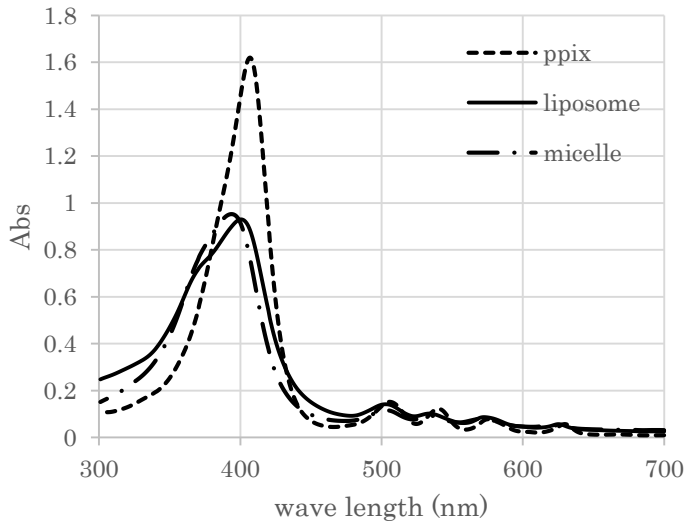

Figure 3. Absorbance of PpIX, PL-C17 micelles, and PL-C17 liposomes. UV/Vis spectra of PpIX, PL-C17 micelles, and PL-C17 liposomes were measured over the 300-700 nm wavelength range in H_2O at 10 μM concentration.

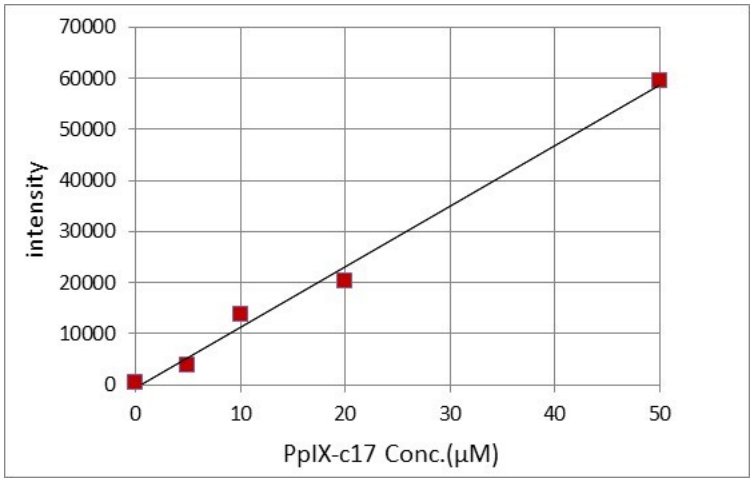

Figure 4. A standard curve of the fluorescence of PL-C17 micelle solution in the 0-50 μM range.

3.2.5. Time-dependent localization and accumulation of PL-C17 micelles and liposomes in cells

Next, I examined the localization of PpIX, PL-C17 micelles and liposomes in HeLa cells and colon 26 cells. The cells were incubated with PL-C17 micelles, liposomes and PpIX for 1-6 h at 100 μM. Fluorescence images of each porphyrin derivative in colon 26 cancer cells were photographed by a fluorescent miscroscopy immediately (Figure 5-1) and 5 h after incubation at 37 ºC in RPMI-1640 medium (Figure 5-3). As shown in Figure 5-1, Each porphyrin derivative distributed in both the membrane and cytoplasm of cells. Interestingly, PL-C17 micelle and liposomes translocated from membrane to a certain organelle in the cells, whereas PpIX stayed in both the membrane and cytoplasm of cells (Figures 5-2 vs. 5-3). Therefore, we examined that Golgi apparatus were stained with green-fluorescence probes (Golgi-ID, a Golgi apparatus-selective dye suitable for live cell) and confirmed whether PL-C17 micelles and liposomes were localized in Golgi apparatus or not. Figure 5-2 shows fluorescence images of PL-C17 liposomes (red) and Golgi apparatus (green) in colon 26 cells. The merged image indicates the orange fluorescence, revealing that the PL-C17 micelles and liposomes are accumulated in the Golgi apparatus after 2 h incubation (Figure 5-4).

In cellular accumulation study of PL-C17 micelle, liposome and PpIX, HeLa cells were incubated with PL-C17 micelle, liposomes and PpIX for 1-6 h at 100 μM cells, removed from the dishes with 0.25 w/v % Tripsin-1 mmol/L EDTA (WAKO), and collected with PBS, and then the fluorescent intensity of the cells was measured by flow cytometry analysis. As shown in Figure 5-5, the cellular uptake of each porphyrin derivative increased along with the incubation time (Figure 5-5 A), besides the each porphyrin derivative in the cells didn’t decrease in 5 h (Figure 5-5 B).

(A)

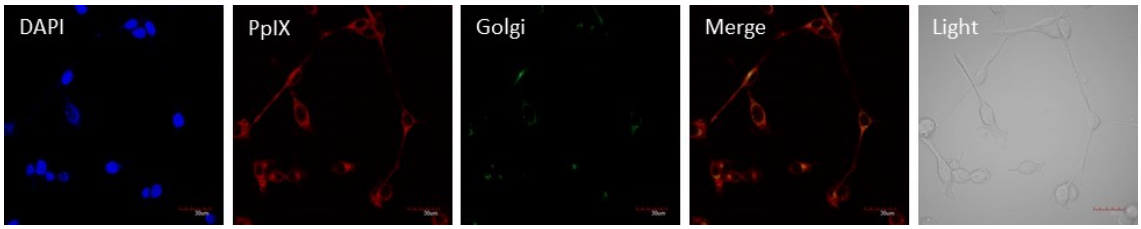

(B)

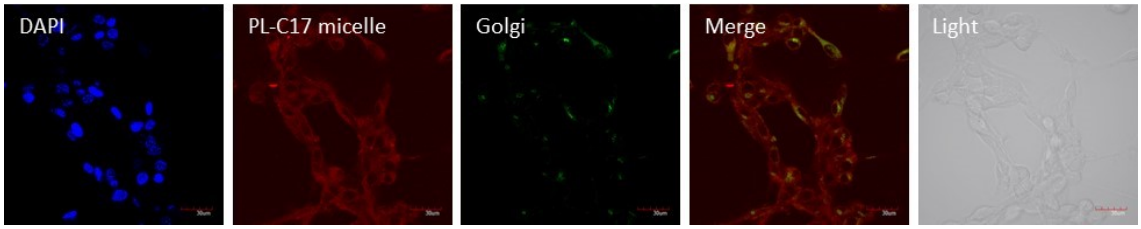

(C)

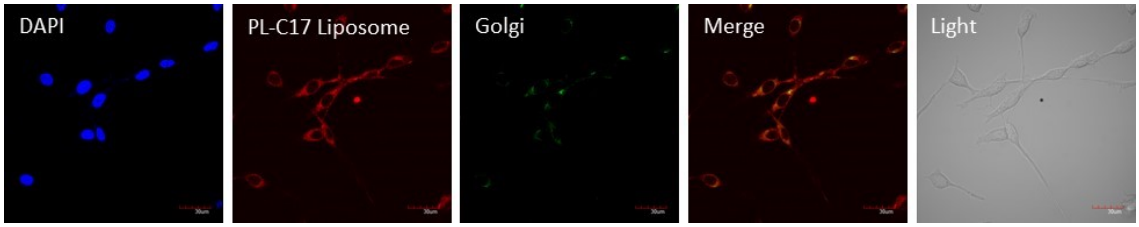

Figure 5-1. Colon 26 cells were incubated with PL-C17 micelles, PL-C17 liposomes, and PpIX for 1h at 100 μM. Fluorescence images of PpIX (A), PL-C17 micelles (B) and PL-C17 liposomes (C) in the cells are visualized immediately by confocal fluorescence microscopy after PBS wash. The cell nuclei were stained with DAPI and Golgie apparatus were stained with Golgi-ID, a Golgi apparatus-selective dye suitable for live cells (Green Assay Kit, Enzo Life Sciences, Inc.). Scale bars indicate 30 μm.

(A)

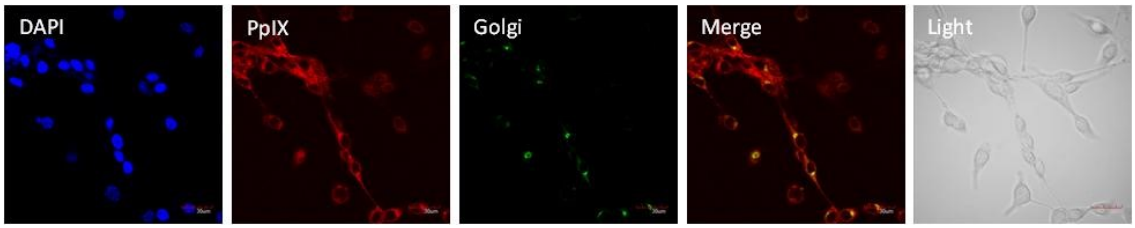

(B)

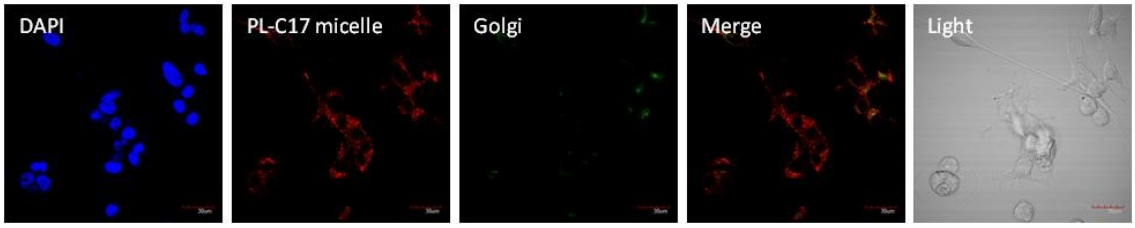

(C)

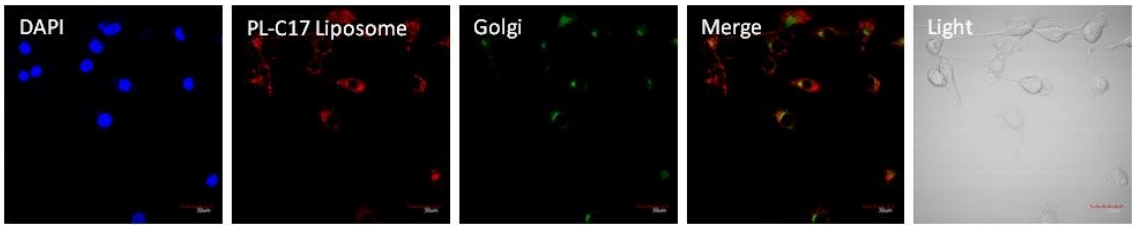

Figure 5-2. CT26 cells were incubated with the cells for 1 h at 100 μM concentration of PPIX or PL-C17 micelle and liposomes. After cells were washed with PBS, the cells incubated 2 h at 37ºCin RPMI-1640 medium. Fluorescence images of PpIX (A) and PL-C17 micelles (B) and PL-C17 liposomes (C) in Colon 26 cells. PL-C17 (red) was visualized with confocal fluorescence microscopy. The cell nuclei were stained with DAPI. Golgies were stained with Golgi-ID, a Golgi apparatus-selective dye suitable for live cell (Green Assay Kit, Enzo Life Sciences, Inc.). Scale bars indicate 30 μm.

(A)

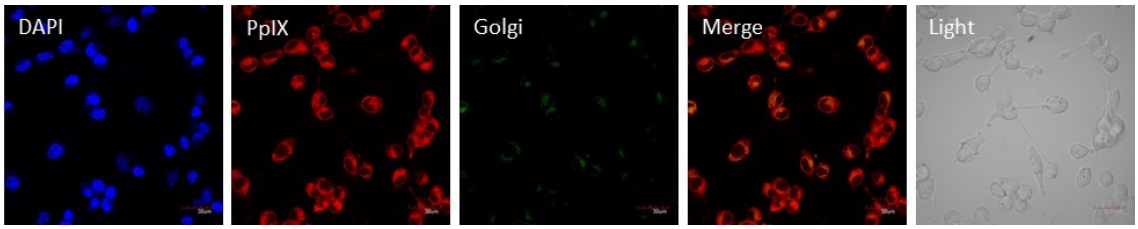

(B)

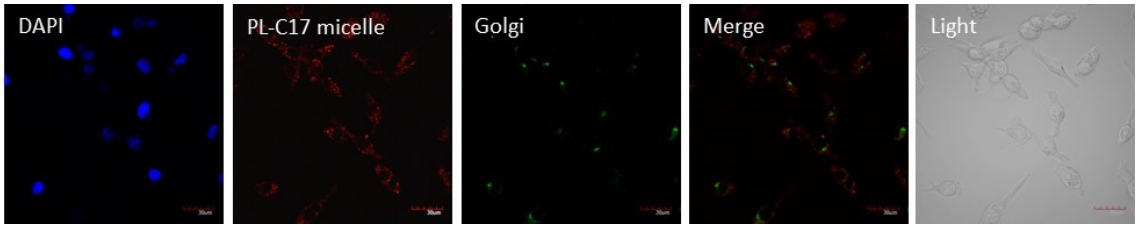

(C)

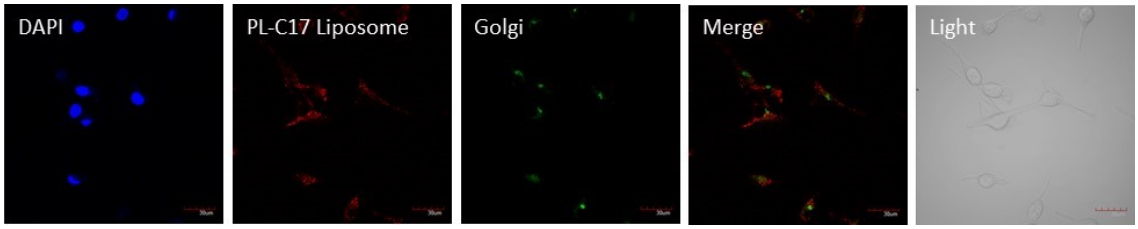

Figure 5-3. Colon 26 cells were incubated with PL-C17 micelle, liposomes and PpIX for 1h at 100 μM. Fluorescence images of each porphyrin in the cells are shown 5h incubated at 37ºCin RPMI-1640 medium after washing each porphyrin. PpIX (A), PL-C17 micelles (B) and PL-C17 liposomes (C). PL-C17 (red) was visualizedwith confocal fluorescence microscopy. The cell nuclei were stained with DAPI. Golgies were stained with Golgi-ID, a Golgi apparatus-selective dye suitable for live cell (Green Assay Kit, Enzo Life Sciences, Inc.). Scale bars indicate 30 μm.

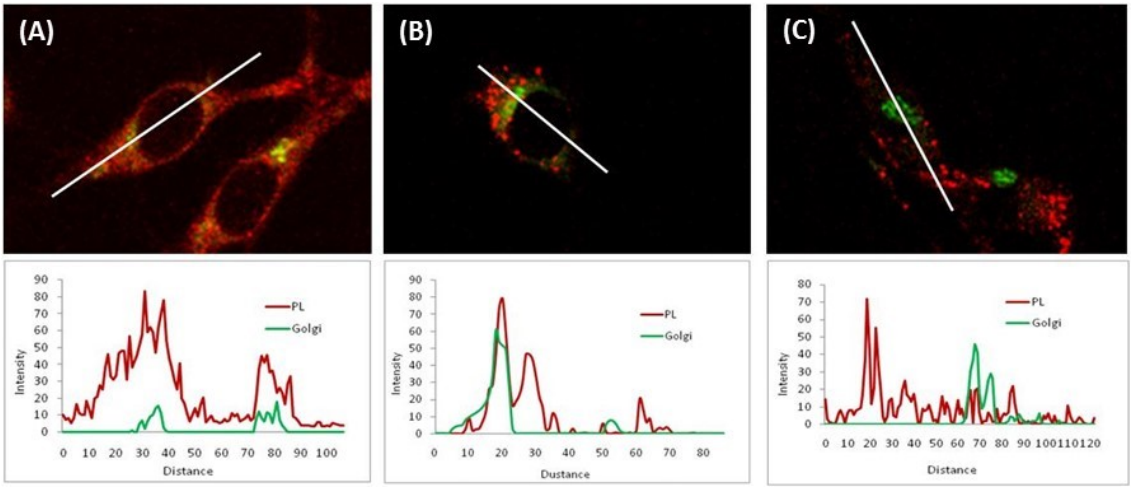

Figure 5-4. Colon 26 cells were incubated with PL-C17 liposomes for 1h at 100 μM. Fluorescence images of each porphyrin in the cells are shown 0h (A), 2h (B) and 5h (C) incubated at 37°C in RPMI-1640 medium after washing each porphyrin. PL-C17 liposome was visualized with confocal fluorescence microscopy. Golgies were stained with Golgi-ID, a Golgi apparatus-selective dye suitable for live cell (Green Assay Kit, Enzo Life Sciences, Inc.).

(A)

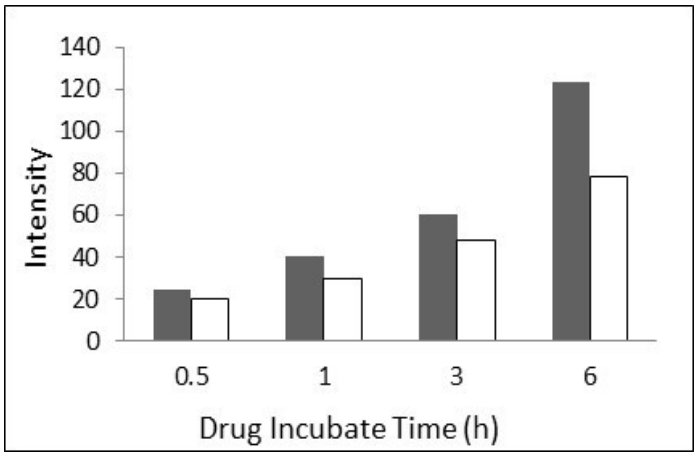

(B)

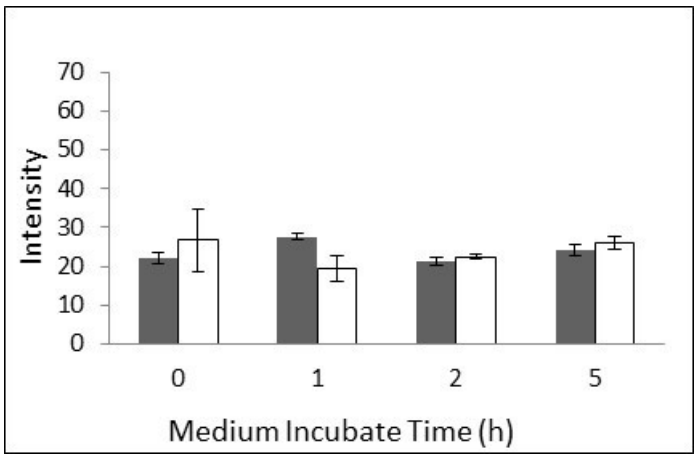

Figure 5-5. Cellular accumlation of PL-C17 micelles (Black bar) and PL-C17 liposomes (White bar) in HeLa cells. The fluorescent intensity was measured by flow cytometry analysis. (A) For timecourse cellular uptake studies, cells were incubated with 100 μM PL-C17 micelle or liposome solution for times ranging from 0.5 to 6 h. (B) For timecourse cellular keeping studies, cell were incubated in medium for times ranging from 0 to 5 h after incubated with 100 μM PL-C17 micelle or liposome solution for 1 h.

3.2.6. Incubation-time dependent PDT effects of PL-C17 micelles and liposomes

Phototoxicity of PL-C17 micelles and liposomes toward HeLa cells was examined under light irradiating conditions. HeLa cells were incubated at 37 ^{o}C for 1 h (Methods A and C) or 6 h (Method B) in RPMI-1640 medium containing various concentrations of the PL-C17 micelles, PL-C17 liposomes or PpIX. Methods A and B: the light irradiation was carried out immediately after removal of the PpIX-lipid micelles-containing medium. Method C: the light irradiation was carried out after removal of the PL-C17 micelles-containing medium followed by 5h incubation in RPMI-1640 medium. (light irradiation; 88 mW/cm^2, 2 min.) After incubation for 72 h, viable cells were determined by MTT assay. The results are summarized in Table 2. PpIX itself significantly inhibited cell growth under light irradiated conditions with IC_{50} of 1.4-4.5 μM. In contrast, the cell growth inhibition of PL-C17 micelles was one-fold less than that of PpIX and IC_{50} was 16.5-17.3 μM as Method A and Method B. PL-C17 liposomes showed approximately twice as potent as PL-17 micelles and the IC50 values were in the range of 6.3-7.9 uM. On the other way, as shown in Table 2. (Method C.), PL-C17 micelles and liposomes indicated the decrease of PDT effect. These results are probably due to more heterogeneous distribution as well as lower absorbance of PL-C17 micelles and liposomes in comparison with PpIX. (Figure 5-2, 3). These results indicates that phototoxicity of PL-C17 micelles and liposomes toward cancer cells is not dependent on their quantity but highly dependent on their localization in the cells. Therfore, next we examined cellular membrane defect on HeLa cells by LDH assay. LDH assay has been widely used to evaluate the damage of tissues and cells. In this study, fifty percent cytopathic damage of HeLa cells incubated with PL-C17 micelle and liposomes for 1 h were about 23.2-35.6 μM (Table 3). On the other hands, cytopathic damage of HeLa cells after 1h incubation with PL-C17 followed by 5 h incubation in RPMI-1640 medium was one–fold less than that after 1 h incubation with PL-C17. These results indicate that PDT effect is highly dependent on the localization of porphyrin derivatives in the cells

Table 2. PDT effect of PpIX, PL-C17 micelles, and PL-C17 liposomes

	Method A	Method B	Method C
PL-C17 Liposome	6.3±1.8	7.9 ±0.9	73.5 ± 4.2
PL-C17 Micelle	17.3±2.2	16.5 ±1.2	> 100
PpIX	3.5 ± 0.1	1.4 ± 0.2	4.5 ±0.7

HeLa cells (5×10^3 cells per well of a 96-well plate) were incubated at 37 ^oC for 1 h (Methods A and C) or 6 h (Method B) in RPMI-1640 medium containing various concentrations of each porphyrin derivative . Methods A and B: the light irradiation was carried out immediately after removal of the PpIX-lipid micelles-containing medium. Method C: the light irradiation was carried out after removal of the PL-C17 micelles-containing medium followed by 5h incubation in RPMI-1640 medium. The cell viability was determined by the MTT assay 72 h after irradiation. The drug concentration required to reduce cell viability by 50% (IC_{50}) was determined from semilogarithmic dose-response plots.

Table 3. LDH Assay toward HeLa cells treated with PpIX, PL-C17 micelles, and PL-C17 liposomes at various concentrations.

50% C.P. (μM)	Method A	Method B
PL-C17 Liposome	23.2	324.6
PL-C17 Micelle	35.6	106.8
PpIX	1.4	4.7

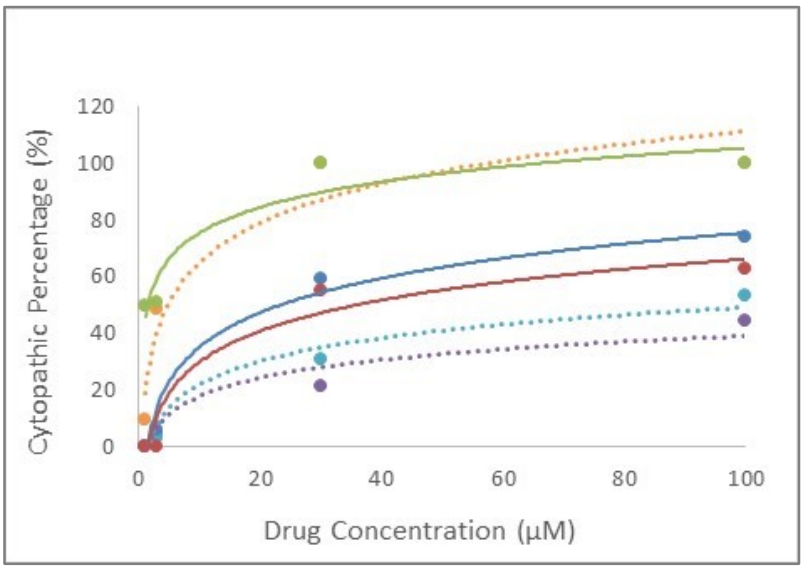

Methods A: the light irradiation was carried out immediately after removal of the each porphyrin derivative-containing medium. Method B: the light irradiation was carried out after removal of the each porphyrin derivative-containing medium followed by 5h incubation in RPMI-1640 medium. HeLa cells were incubated for 1h with PL-C17 micelles(●), PL-C17 liposomes (●), or PpIX (●), and followed by 5 h in RPMI-1640 medium with PL-C17 micelles(●), PL-C17 liposomes (●), or PpIX (●).

3.2.7. Detection of reactive oxygen species (ROS)

The production of reactive oxygen species (ROS) is crucial for efficient PDT. It has been studied that the first ROS formed during PDT is singlet molecular oxygen ($^1O_2$) and that other ROS are formed downstream including superoxide anion radical ($\bullet CO_2^-$), hydrogen peroxide (H_2O_2) and hydroxyl radical (•OH). [22] Therefore, we next examined intracellular ROS imaging and assay generated by PL-C17 micelles and liposomes in cells after light irradiation. Detection of ROS was investigated by molecular green fluorescent probe CM-H_2DCFDA. Figure 6A and 6B show intracellular ROS imaging. The generation of ROS was dependent on concentration of PL-C17 micelles and PL-C17 liposomes in the cells after the light irradiation for 2 min. Both PL-C17 micelles and liposomes effectively induced the ROS in HeLa cells. The ROS production induced by PL-C17 micelles and liposomes resulted in inhibition of the cell growth as indicated in Table 2.

Furthermore, these results displayed that not the quantity but localization of PL-C17 is essential for cytototoxicity induced by ROS in the cells. Next, we examined HeLa cells were incubated with 100 μM PL-C17 micelle or liposome solution for 1 h and after PBS wash incubated in RPMI-1640 medium for times ranging from 0 to 5 h. After irradiation, the intensity of DCF into HeLa cells measured by fluorescence plate reader. As shown in Figure 7, the fluorescence intensity of DCF measured similar over time, respectivery. The results indicated there is no correlation between the amount of ROS and PDT effects, the most important of PDT effect toward cells is localization of ROS generated from PL-C17 micelle and liposmes in cell membrane. (Table 3)

(A)

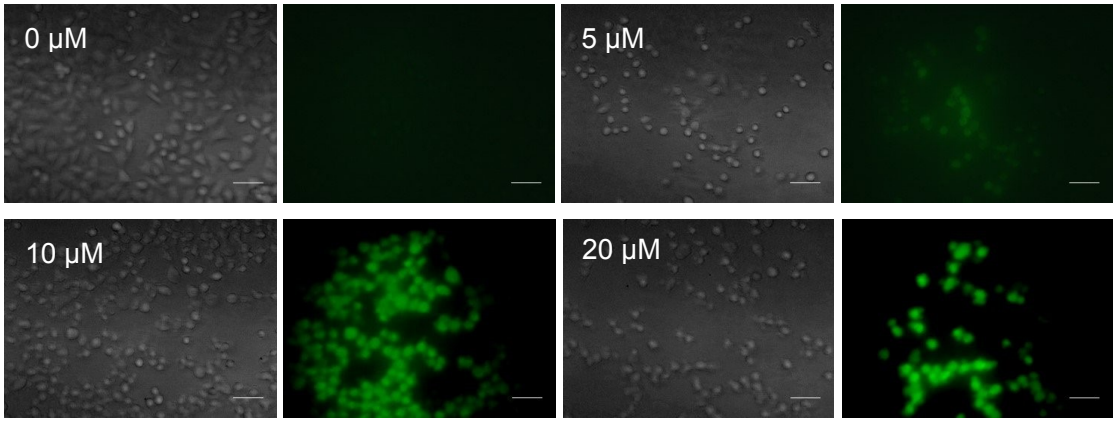

(B)

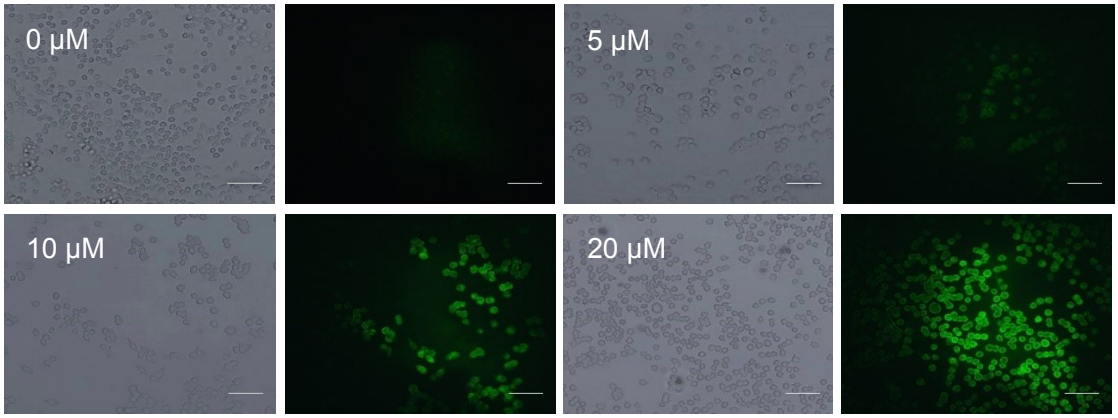

Figure 6. Concentration-dependent generation of reactive oxygen species (ROS) after the light irardiation with a xenon lamp in the 400 to 800 nm range for 2 min. in the presence of PL-C17 micelles (A) and PL-C17 liposomes (B). After PBS washes, cells were stained with H_2DCFDA (10μM) for 30 min. Scale bars indicate 40 μm.

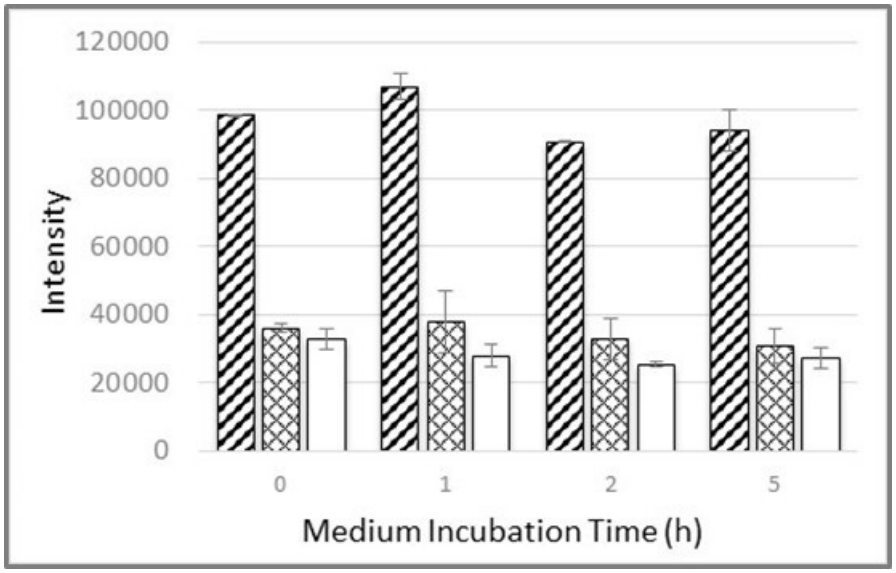

Figure 7. The generation of reactive oxygen species (ROS) after irradiation with a xenon lamp in the 400–800 nm range for 2 min in the presence of PpIX (slash bar), PL-C17 micelles (cross bar) and PL-C17 liposomes (white). After irradiation, the cells were cultured in RPMI-1640 for 0-5 h and stained with H2DCFDA (10 μM) for 30 min. The cells were lysed and then the fluorescent intensity was measured by fluorescence plate reader (Thermo Fisher). None (no drug and irradiation) was used as a positive control.

3.2.8. ROS-induced oxidation of DOPC with in PL-C17 micelle solution

PL-C17 micelle solution was added to a methanol solution of DOPC (dioleoylphosphatidylcholine) and the mixture was stirred for 1 min. Then, the mixture was irradiated with a xenon lamp in the 400–800 nm range for 2 min. and Mass Spectra of the mixture was measured by LCMS (Shimadzu). The Mass spectra of the mixture appeared at 817.6 and 850.6, that were assigned the adducts of two and four oxygen atoms to DOPC, respectively. The result indicated singlet oxygen oxidized to double bond with DOPC. [23]

(A)

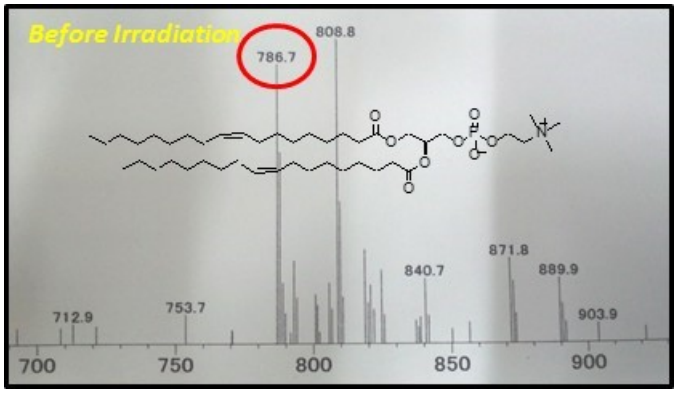

(B)

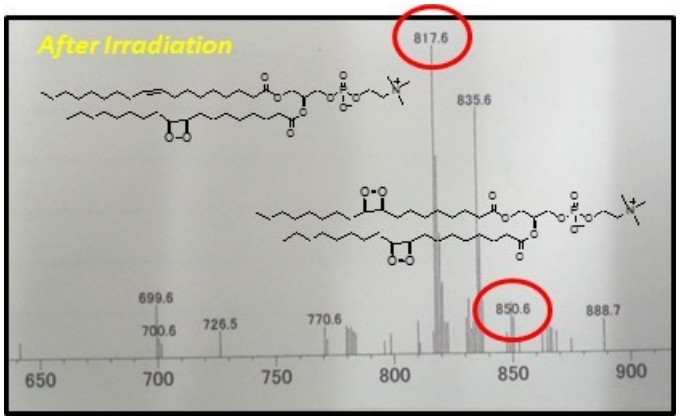

]

Figure 8. Mass spectra of the mixture of DOPC and PL-C17 micelle in methanol before (A) and after (B) light irradiation.

3.2.9. Ros-induced disruption of calcein-encapsulating DOPC liposomes post-inserted with PL-C17 as a cell membrane model

As a cell membrane model, the liposomes were prepared from DSPC, DOPC, cholesterol and DSPE-PEG (0.75:0.25:0.1:0.11, molar ratio) in a 100 mM calcein solution by the reverse-phase evaporation (REV) method. PL-C17 micelle solution (Phosphatidylcholine : PL-C17= 1 : 0.1) was added to the liposome solution to generate calcein-encapsulating DOPC liposomes with PL-C17 (the post-inserted liposomes). The liposome were irradiated with a xenon lamp (88 mW/cm^2, average) in 96-well plate in the 400–800 nm range for 2 min, and the intensity of released calcein was measured at 0, 30, 90, and 180 min after irradiation by fluorescence plate reader. As shown in Figure 8, the intensity of the calcein-encapsulating liposome with PL-C17 irradiated (●) increased in a time-dependent manner, whereas the intensity of the liposome treated with 1% triton x100 (○) and control (without irradiation) did not increased. The intensity of calcein released from the liposome was similar to that treated with 1% triton x100 at 150 min after irradiation. Furthermore, the average particle size of calcein-encapsulating liposome post-inserted with PL-C17 was changed from 126.8 nm to 164.7 nm after light irradiation (Figure 9). These results indicated that oxidization of double bond in DOPC ruptured the liposomal membrane and calcein was released from the inner of the liposomes, revealing that the rupture of cell membrane by addition of single oxygen may induce additional effects of phototoxicity toward cancer cells.

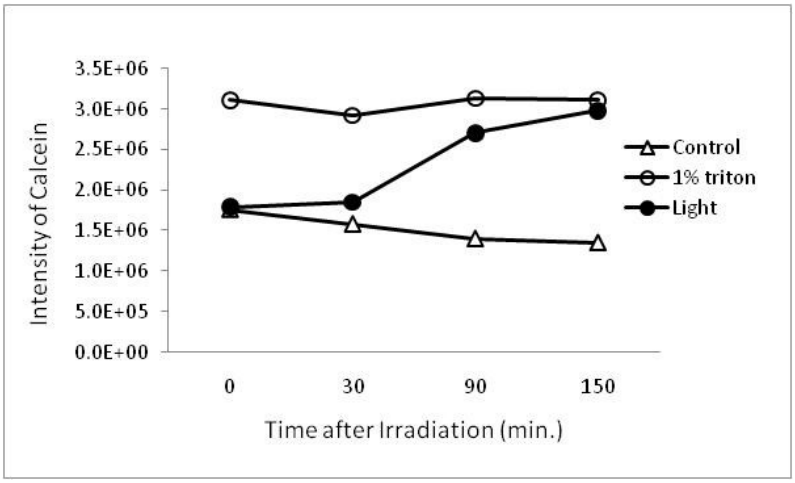

Figure 9. Intencity of calcein release from calcein encapsulated liposome with PL-C17 after irradiation. ○, 1% triton X100; ●, with irradiation; △, Control (without irradiation)

(A)

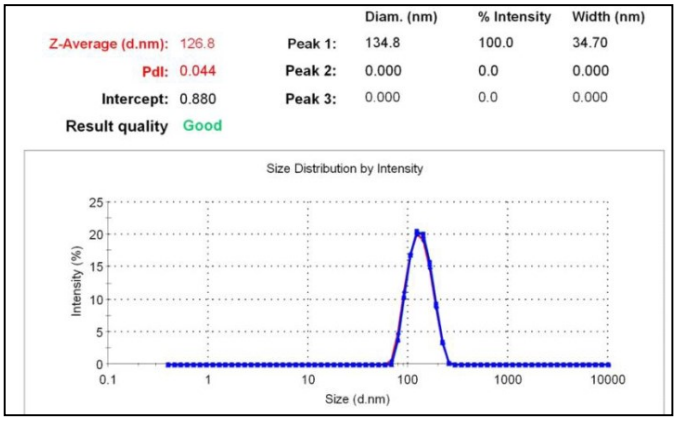

(B)

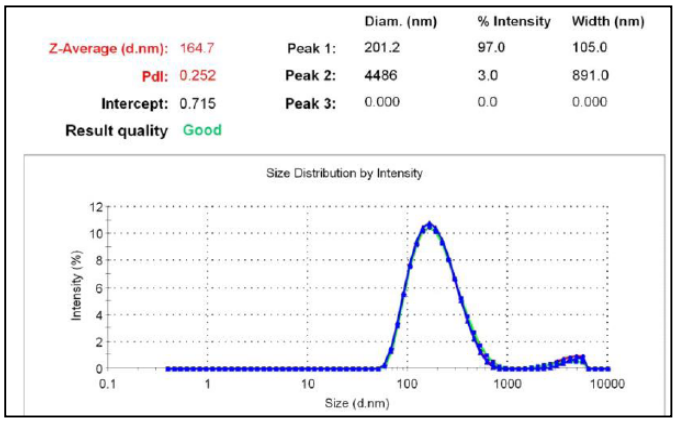

Figure 10. Particle size of encapsulating DOPC liposome with PL-C17 (A) before (B) after irradiation

3.2.10. Biodistribution of PL-C17 micelles and liposomes in colon 26 tumor bearing mice

PL-C17 micelles and liposomes were injected into the colon 26 tumor bearing mice via the tail vein and the tumor tissue section was prepared for their biodistribution analysis by a fluorescence microscopy. Because of the poor water-solubility of PpIX, 5-aminolevulinicacid (5-ALA) was used as a control experiment. It is known that 5-ALA is converted to PpIX in biosynthetic pathway, thus 5-ALA has been used for PDT and photodiagnosis. [23] Fluorescence images of the tumor tissue of mice 36 h after injection of PL-C17 micelles and liposomes are shown in Figure 5A and 5C, respectively, and each tissue section stained with HE (Hematoxylin-Eosin) is shown in Figure 5B and 5D, respectively. Although the red fluorescence was observed in the tumoral tissue of mice injected with PL-C17 micelles (Figure 5A), the stronger fluorescence was detected in those injected with PL-C17 liposomes (Figure 5C). On the other hand, the fluorescence of PpIX derived from 5-ALA by *in vivo* biosynthesis was not clearly observed in Figure 5E. These results indicate that the PL-C17 liposome is an effective delivery vehicle of PpIX-based photosensitizers to tumor *in vivo*.

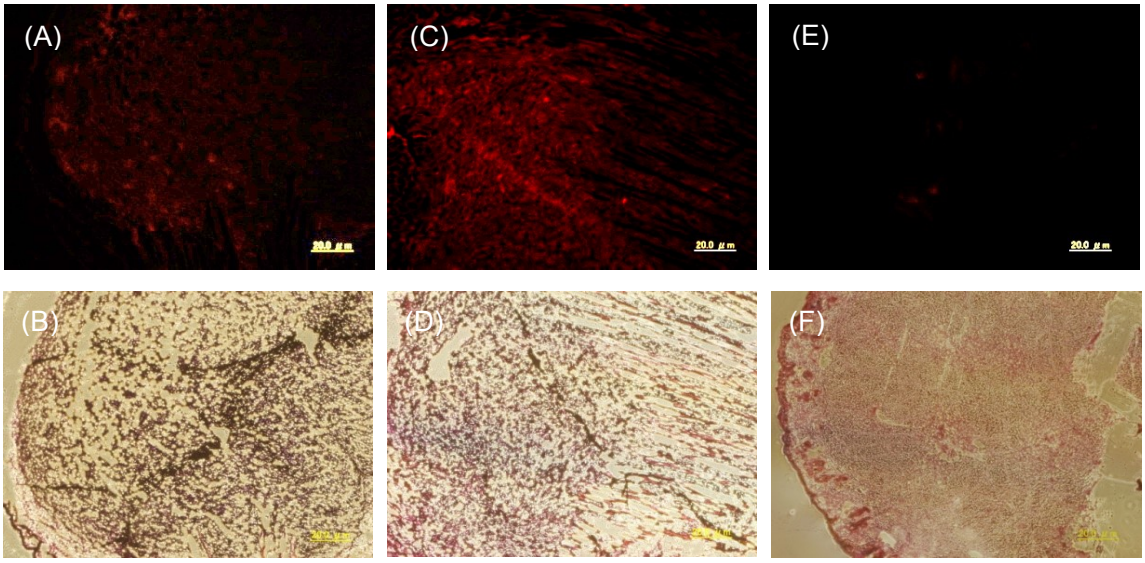

Figure 11. Biodistrubution of PL-C17 micelles (A) and PL-C17 liposomes (C) in colon 26 tumor bearing mice. 5-ALA was used a control experiment (E). (B), (D), and (F) show each tissue section stained with hematoxylin-eosin (HE), respectively.

3.3. Conclusion

PpIX lipids (PL) were synthesized by attaching two long alkyl chain, such as C13, C15, and C17, on PpIX. The PpIX lipids having amphiphilic property are water soluble by forming their micelle formations in water and relatively low cytotoxic toward colon 26 cells (IC_{50} = 151.7 – 379.9 μM) without light irradiation. PL-C17 liposomes were readily prepared by post-insertion of PL-C17 into outer membrane of the liposomes. PL-C17 micelles homogeneously-dispersed on membrane of the liposomes prevent the aggregation of porphyrins that is considered to diminish the PDT effect. These PL-C17 micelles, liposomes and PpIX distributed in the membrane and cytoplasm of cells 1 h after incubation. However, PL-C17 micelles and liposomes were translocated into Golgi apparatus after 2h and into a certain organelle in the cells after 5 h, whereas PpIX was located in the both membrane and cytoplasm. Furthermore, PDT effect of each porphyrin derivative on HeLa cells was highly dependent on the intracellular localization. A significant cytotoxicity was observed in the porphyrin derivatives localized in plasma membrane, whereas low cytotoxicity was observed in the porphyrin derivatives accumulated into the cytoplasm. In order to clarify the mechanism of phototoxicity, we examined the LDH assay to analyze cellular membrane defect. LDH assay has been widely used to evaluate the presence of damage and toxicity of tissue and cells, Cytopathic damage of the cell membrane is highly dependent on the localization of porphyrin derivatives. Furthermore, the intracellular ROS generation was detected by molecular green fluorescent probe CM-H_2DCFDA, revealing that the localization of porpyrin derivatives is more important than the accumulation for the PDT effect on HeLa cells. Indeed, the experiment using calcein-encapsulating DOPC liposome with PL-C17 for the cell membrane model suggested the possibility of phototoxicity caused by disruption of cellular membrane by the oxidation of unsaturated phospholipids by ROS.

Finally, PL-C17 liposomes were observed in tumor tissue 36 h after *i.v.* administration in tumor-bearing mice. Since PL-C17 liposomes are still vacant in their interior aqueous core, drugs including photosensitizers or antitumor agents are able to be encapsulated in

the liposomes. In this regard, we can envision the combination therapy of PDT and chemotherapy using the current photosensitizer lipid liposome system.

3.4. Materials and Methods

3.4.1. General.

^{1}H NMR and ^{13}C NMR spectra were measured with Jeol JNM-AL 300 (300 MHz) and Varian Unity-Inova 400(400 MHz) spectrometers. ^{1}H NMR and ^{13}C NMR chemical shifts are expressed in parts per million (ppm, δ units), and coupling constants are expressed in hertz (Hz). IR spectra were measured with a Shimadzu FTIR-8200 A spectrometer. UV/Vis spectra were measured with a Shimadzu 2450 PC spectrophotometer over the300–700 nm wavelength range. Elemental analyses were performed with a Perkin–Elmer 2400 automatic elemental analyzer. The fluorescence (excitation and emission) spectra were determined with a Jasco FP-6500 PC spectrophotometer. Electron spray ionization (ESI) mass spectra were recorded with a Shimadzu LCMS-2010 eV spectrometer. Analytical thin-layer chromatography (TLC) was performed on glass plates (Merck Kieselgel 60 F254, layer thickness 0.2 mm). Samples were visualized with the aid of UV light (254 nm), I_2, or $KMnO_4$. Column chromatography was performed on silica gel (Merck Kieselgel 70–230 mesh). Preparative thin layer chromatography (TLC) was carried out with 0.75 mm layers ofsilica gel G (Merck, GF254) made from water slurries on glass plates of dimensions 20×20 cm^2, followed by drying in air at 100^{o}C. All reactions were performed with shielding from light in dry solvents under nitrogen atmosphere using standard Schlenk techniques. Distearoylphosphatidylcholine (DSPC), Dioleylphosphatidylcholine (DOPC) and DSPE-PEG (SUNBRIGHT DSPE-020CN) were purchased from Nippon Oil and Fats (Tokyo, Japan).All chemicals were of analytical grade and were used without further purification.

3.4.2. Synthesis of PpIX Lipids

Dimethyl 3,3'-(7,12-bis(1-tridecanoxyethyl)-3,8,13,17-tetramethylporphyrin-2,18-diyl)dipropionate (3a).

Compound **1** (590 mg, 1.0mmol), which was prepared from protoporphyrin IX (PpIX) under acid esterification condition, [24] was dissolved in HBr/acetic acid (25%, 30 mL) under nitrogen atmosphere and the mixture was stirred for 2 h. All volatile solvents were evaporated under vacuum to yield dimethyl 3,30-(7,12-bis(1-bromoethyl)-3,8,13,17-tetramethylporphyrin-2,18-diyl)dipropionate (2) as a green colored liquid. The resulting liquid was directly dissolved in dichloromethane (50 mL), and 1-tridecanol(2.2 mmol, 441 mg) and Cs2CO3 (2.2 mmol, 304 mg) were added to the dichloromethane solution. The reaction mixture was again stirred under nitrogen atmosphere for 2 h and filtered. The resulting filtrate was concentrated under the reduced pressure and the residue was purified by preparative TLC on silica gel with CH2Cl2/MeOH (20:1) to give compound **3a** (218 mg, 23% yield) as a dark violet crystal. Rf= 0.8 (CH_2Cl_2/MeOH 20:1); 1H NMR(400 MHz, $CDCl_3$, TMS) δ10.63 (s, 1H), 10.61 (s, 1H), 10.11 (s,1H), 10.08 (s, 1H), 6.09 (m, 2H), 4.41–4.45 (m, 4H), 3.73 (s, 3H),3.71 (s, 3H), 3.70 (s, 3H), 3.69 (s, 3H), 3.68 (s, 3H) 3.67 (s, 3H), 3.65 (m, 4H), 3.28–3.32 (m, 4H), 2.25–2.27 (d, J = 7.0 Hz, 6H),1.09–1.80 (m, 42H), 0.84 (t, J = 12.9 Hz, 6H); 13C NMR (75 MHz,$CDCl_3$, TMS) δ173.7 (2C; C=O), 140.6, 140.4, 138.4, 138.2, 137.2,136.8, 136.5 (16C; C pyrrole), 98.8, 98.6, 96.8, 96.1, 73.3 (2C,OCH) 69.6 (2C, OCH_2), 51.74 (2C; CO_2CH_3), 37.0 (2C, CH_3CH), 31.9(2C; CH_2COOMe), 30.3, 29.5, 29.3, 26.4, 25.5, (24C; -CH_2-), 22.6(2C; CH_2CH_2COO), 21.9, 14.1 (2C, CH_3C pyrrole), 11.7 ppm (2C;CH_3C pyrrole); IR (NaCl disc) 3311, 2924, 2853, 1739, 1435,1100 cm^{-1}; MS (ESI, positive): m/z (%): 991; HRMS (ESI, positive)m/z Calcd for $C_{62}H_{94}N_4O_6$ [M+H]+; 991.7252, found: 991.7252.

Dimethyl 3,3'-(7,12-bis(1-pentadecanoxyethyl)-3,8,13,17-tetramethylporphyrin-2,18-diyl)dipropionate (3b).

This compound was synthesized from compound **1** (590 mg,1.0 mmol) and 1-pentadecanol (503 mg, 2.2 mmol) using the procedure described for **3a** to give **3b** (200 mg 18% yield) as a dark violet solid: Rf= 0.8 (CH_2Cl_2/MeOH 20:1); 1H NMR (400 MHz, $CDCl_3$,TMS) δ10.61 (s, 1H), 10.59 (s, 1H), 10.10 (s, 1H), 10.07 (s, 1H), 6.10 (m, 2H), 4.40–4.44 (m, 4H), 3.71 (s, 3H), 3.70 (s, 3H), 3.69 (s,3H), 3.68 (s, 3H), 3.67 (s, 3H), 3.65 (s, 3H), 3.64 (m, 4H), 3.27–3.31 (m, 4H), 2.24–2.25 (d, J = 3.4 Hz, 6H), 1.07–1.80 (m, 50H),0.84 (t, J = 7.0 Hz, 6H; CH3); 13C NMR (75 MHz, $CDCl_3$, TMS) δ173.6 (2C; C=O), 140.4, 138.3, 137.3, 137.0 (16C; C pyrrole), 98.8,98.5, 96.8, 96.1, 73.3 (2C; OCH), 69.6 (2C; OCH_2), 51.7 (2C;$COOCH_3$), 37.0, 31.9 (2C; CH_2COOMe), 30.3, 29.6, 29.5, 29.3 26.4,25.5 (26C; -CH_2-), 22.7 (2C;CH_2CH_2COOMe), 21.9 (2C;-CH_2-),14.1 (2C; CH_3C pyrrole), 11.8 (2C; CH_3C pyrrole) ppm; IR (NaCl disc) 3311, 2923, 2853, 1739, 1457, 1166 cm^{-1}; MS (ESI, positive):m/z (%): 1047; HRMS (ESI, positive) m/z Calcd for $C_{66}H_{102}N_4O_6$[M+H]+; 1047.7878, found: 1047.7878.

Dimethyl 3,3'-(7,12-bis(1-heptadecanoxyethyl)-3,8,13,17-tetramethylporphyrin-2,18-diyl)dipropionate (3c).

This compound was synthesized from compound **1** (590 mg,1.0 mmol) and 1-heptadecanol alcohol (564 mg, 2.2 mmol) using the procedure described for **3a** to give **3c** (210 mg 21% yield) as a dark violet solid: Rf= 0.8 (CH_2Cl_2/MeOH 20:1); 1H NMR(400 MHz, $CDCl_3$, TMS) δ10.62 (s, 1H), 10.60 (s, 1H), 10.11 (s, 1H),10.07 (s, 1H), 6.08 (m, 2H), 4.04–4.44 (m, 4H), 3.74 (s, 3H), 3.72(s, 3H), 3.70 (s, 3H), 3.69 (s, 3H), 3.68 (s, 3H), 3.67 (s, 3H), 3.65(m, 4H), 3.28–3.31 (m, 4H), 2.24–2.26 (d, J = 6.4 Hz, 6H), 1.08–1.77 (m, 58H), 0.86 (t, J = 6.8 Hz, 6H; CH_3); 13C NMR (75 MHz, $CDCl_3$, TMS) δ173.6 (2C; C=O), 140.4, 138.3, 137.1, 136.7 (16C; C pyrrole), 98.82, 98.54, 97.73, 96.04, 73.3 (2C;

OCH), 69.6 (2C;OCH_2), 51.7 (2C; $COOCH_3$), 36.9, 31.9 (2C; CH2COOMe), 30.3, 29.7,29.6, 29.6, 29.5, 29.5, 29.3, 26.4, 25.5 (30C; -CH_2-), 22.7 (2C;CH_2CH_2COOMe), 21.9 (2C;-CH_2-), 14.1 (2C; CH_3C pyrrole), 12.5(2C; CH_3C pyrrole) ppm; IR (NaCl disc): 3311, 2924, 2852, 1739,1435, 1166 cm^{-1}; MS (ESI, positive): m/z (%): 1103; HRMS (ESI, positive) m/z Calcd for $C_{70}H_{110}N_4O_6$ [M+H]+; 1103.8504, found:1103.8504.

3,3'-(7,12-Bis(1-tridecanoxyethyl)-3,8,13,17-tetramethylporphyrin-2,18-diyl)dipropionic acid(4a: PL-C13).

Compound **3a** (99.1 mg, 0.1 mmol) was dissolved in a THF/MeOH/H2O mixture (15 mL, 1:1:1). LiOH•H_2O (9.23 mg, 0.22mmol) was added and the reaction mixture was stirred for6 h at room temperature. The reaction mixture was filtered and the volume of the filtrate was reduced under vacuum (5 mL). HCl (1 N, 2 mL) was slowly added to this solution with stirring to precipitate the dark violet solid, which was filtered off and the washed with water (5 mL) to give **4a** (86.8 mg, 90% yield) as a dark violet solid. Rf= 0.8 (CH_2Cl_2/MeOH 20:1); 1H NMR (400 MHz,$CDCl_3$, 25 _C, TMS) δ10.67 (br s, 1H), 10.65 (br s, 1H), 10.11 (br s,2H), 6.08 (m, 2H), 4.45 (m, 4H), 3.73 (s, 3H), 3.69 (s, 3H), 3.67 (s,3H) 3.65 (s, 3H), 3.63 (m, 4H), 3.36–3.37 (m, 4H), 2.23–2.24 (d, J = 2.4 Hz, 6H), 1.08–1.80 (m, 42H), 0.83 (t, J = 7.0 Hz, 6H); 13CNMR (300 MHz, $CDCl_3$, TMS) δ179.6 (2C; C=O), 145.2, 140.8,140.1 (16C; C pyrrole), 99.2, 98.8, 97.2 (4C; porphine), 73.3 (2C,OCH), 69.6 (2C, OCH_2), 37.5 (2C, CH_3CH), 31.8 (2C; CH_2COOMe),30.3, 29.7, 29.5, 29.3, 26.4, 25.5 (24C; -CH_2-), 22.6 (2C; CH_2CH_2COO), 14.1 (2C, CH_3C pyrrole), 11.7 ppm (2C; CH_3C pyrrole); IR (NaCl disc): 3309, 2923, 2853, 1713, 1456, 1100 cm^{-1};MS (ESI, positive): m/z (%): 963.7; HRMS (ESI, positive) m/z Calcd for $C_{60}H_{90}N_4O_6$ [M+H]+; 963.6939, found: 963.6939.

3,3'-(7,12-Bis(1-pentadecanoxyethyl)-3,8,13,17-tetramethylporphyrin-2,18-diyl)dipropionic acid (4b: PL-C15).

This compound was synthesized from compound **3b** (105.0 mg,0.1 mmol) and LiOH•H_2O(9.23 mg, 0.22 mmol) using the procedure described for **4a** to give **4b** (91.8 mg, 90% yield) as a dark violet solid; Rf= 0.8 (CH_2Cl_2/MeOH 20:1); 1H NMR (400 MHz, $CDCl_3$,TMS) δ10.67 (br s, 2H), 10.11 (br s, 2H), 6.10 (m, 2H), 4.43 (m, 4H), 3.74 (s, 3H), 3.72 (s, 3H), 3.68 (s, 3H), 3.66 (s, 3H), 3.62 (m,4H), 3.34 (m, 4H), 2.24 (m, 6H), 1.09–1.78 (m, 50H), 0.83–0.87(m, 6H); 13C NMR (300 MHz, $CDCl_3$, TMS) δ179.9, 179.6 (2C;C=O), 140.8, 138.0, 136.7 (16C; C pyrrole), 99.2, 98.8, 97.2, 95.7(4C; porphine), 73.3 (2C; OCH), 69.6 (2C; OCH_2), 37.5 (2C, CH_3CH),31.9 (2C; CH_2COOMe), 30.3, 29.7, 29.5, 29.6, 29.3, 26.4, 25.5 (26C; -CH_2-), 22.7 (2C; CH_2CH_2COOMe), 22.0 (2C; -CH_2-), 14.1 (2C; CH_3Cpyrrole), 11.7, 11.6 (2C; CH_3C pyrrole) ppm; IR (NaCl disc): 3311,2923, 2853, 1739, 1455, 1165 cm^{-1}; MS (ESI, positive): m/z(%):1019; HRMS (ESI, positive) m/z Calcd for $C_{64}H_{98}N_4O_6$ [M+H]+; 1019.7565, found: 1019.7568.

3,3'-(7,12-Bis(1-heptadecanoxyethyl)-3,8,13,17-tetramethylporphyrin-2,18-diyl)dipropionic acid(4c: PL-C17).

This compound was synthesized from compound **3c** (110 mg,0.1 mmol) and LiOH•H_2O (9.23 mg, 0.22 mmol) using the procedure described for **4a** to give **4c** (100 mg, 93% yield) as a dark violet solid; Rf= 0.8 (CH_2Cl_2/MeOH 20:1); 1H NMR (400 MHz, $CDCl_3$, TMS)δ10.67 (br s, 1H), 10.65 (br s, 1H), 10.12 (br s, 1H), 10.10 (br s, 1H),6.12 (m, 2H), 4.45–4.51 (m, 4H), 3.77 (s, 3H), 3.75 (s, 3H), 3.73 (s,3H), 3.70 (s, 3H), 3.64 (m, 4H), 3.41–3.42 (m, 4H), 2.24–2.27 (m,6H), 1.10–1.84 (m, 58H), 0.85–0.90 (m, 6H); 13C NMR (300 MHz,$CDCl_3$, TMS) δ180.1 (2C; C=O), 140.6, 137.9, 137.0, 136.5 (16C; C pyrrole), 99.1, 98.8, 96.9, 95.5 (4C; porphine), 73.3 (2C; OCH),69.6 (2C; OCH_2), 37.6 (2C,

CH_3CH), 31.9 (2C; CH_2COOMe), 30.3,30.2, 29.7, 29.6, 29.5, 29.3, 26.5, 26.4, 25.5, 25.4 (30C; -CH_2-), 22.7 (2C; CH_2CH_2COOMe), 22.0 (2C; -CH_2-), 14.1 (2C; CH_3C pyrrole),11.8 (2C; CH_3C pyrrole) ppm; IR (NaCl disc): 3311, 2923,2852, 1709, 1463, 1099 cm^{-1}; MS (ESI, positive): m/z (%):1075;HRMS (ESI, positive) m/z Calcd for $C_{70}H_{106}N_4O_6$ [M+H]+;1075.8191, found: 1075.8183.

3.4.3. Preparation and characterization of PpIX-lipid micelle

PpIX-lipids (PL-C13, PL-C15, or PL-C17; 0.01 mmol) dissolved in THF and methanol solution (4 mL, THF : methanol = 3 :1) was added to an aqueous lithium hydroxide solution (0.02 M, 1mL) and the mixture was stirred for 1h. THF was removed under the reduced pressure and the resulting lithium salts (**5a-c**) of PpIX-lipids were dissolved in water (1mL) to form micelles. PpIX lipids micelle solution was filtrated 3 times through a filter with 0.45 μm pore size (Sigma Aldrich, 16555K, Minisart Filter, 0.45μm). Particle sizes of these micelles were measured with an electrophoretic light scatteringspectrophotometer (Nano-ZS, Sysmex, Japan). UV/Vis spectra were measured with a Shimadzu 2450 PC spectrophotometer over the 300–700 nm wavelength range.

3.4.4. Cytotoxicity of PpIX-lipid micelles without light irradiation

Human cervical carcinoma HeLa cells were used for these cell viability assay. These cells (5×10^3 cells per well of a 96-well plate) were incubated at 37 ^oC for 72 h in RPMI-1640 medium (100 μL) containing various concentrations of the PpIX-lipid micelles. After the incubation, 3'-(4,5-dimethylthiazol-2-yl)-2,5-diphenyltetrazolium bromide (MTT, Sigma) in PBS (5 mg/mL, 10μL) was added to each well, and the cells were further incubated at 37 ^oC for 2h. After the removal of the medium, DMSO (100 mL) was added and the absorbance at 570 nm was determined with a microplate reader. The drug

concentration required to reduce cell viability by 50% (IC_{50}) was determined from semilogarithmic dose-response plots.

3.4.5. Preparation and characterization of PL-C17 liposomes

Polyethyleneglycol (PEG)-liposomes were prepared from DSPC, Cholesterol and DSPE-PEG (1:1:0.11, molar ratio) by thereverse-phase evaporation (REV) method. [25] Briefly, amixture of DSPC (158mg, 0.2mmol), cholesterol (77.3mg, 0.2 mmol), and DSPE-PEG (63.8mg, 0.02mmol) were dissolved in 5mL of chloroform/ diisopropylether mixture (1:1, v/v) in a round-bottom flask. Saline was added to the lipid solution to form an emulsion. The emulsion was sonicated for 3 min., and then, the organic solvent was removed under vacuum in a rotary evaporator at 55 ^{o}C for 30 min. to obtain a suspension of liposomes. The liposomes obtained were subjected to extrusion 10 times through a polycarbonate membrane of 100 nm pore size (Whatman, 110605, FILTER, 0.1UM, 25MM, Gentaur Molecular Products, Belgium), using an extruder device (LIPEX^{TM} Extruder, Northern Lipids, Canada) thermostated at 55 ^{o}C. Purification was accomplished by ultracentrifuging at 200,000 g for 60 min. at 4 ^{o}C (himac cp 80 wx, Hitachi Koki, Japan), and the pellets obtained were resuspended in saline. PL-C17 micelle solution (DSPC : PL-C17= 1 : 0.05-0.2 molar ratio) was added to the liposome solution to generate PL-C17 liposomes (the postinserted liposomes). Purification was accomplished by ultracentrifuging at 200,000 g for 60 min at 4 ^{o}C, and the pellets obtained were resuspended in saline. Particle size and zeta potential of PL-C17 liposomes were measured with the electrophoretic light scatteringspectrophotometer. The concentartion of PL-C17 post-inserted into PEG-Liposome was determined by a standard curve of PL-C17 fluorescence. Fluorescence is linearly proportional to dye concentration in dilute samples. However, if the concentration is too high self-quenching occurs and the relationship between fluorescence and concentration is not linearly.

3.4.6. Time-dependent localization and accumulation of PL-C17 micelles and liposomes in cells

HeLa cells and colon 26 cells (1×10^4 cells) plated on 35 mm glass bottom dishes were incubated either with PL-C17 micelles, PL-C17 liposomes or PpIX at 100 μM concentration for 1-6 h. After cells were washed with PBS, the cells were cultured in RPMI-1640 medium for 0-5 h, fixed with paraformaldehyde (4%) for 15 min., and stained with 4',6-diamidino-2-phenylindole (DAPI; 100 nM) and Golgi-ID (50 nM, Green Assay Kit, Enzo Life Sciences, Inc.) for 10 min. The cells were observed and photographed with an Olympus IX71 microscope. To quantify the intracellular concentration of PL-C17 micelle and liposome, cells were washed with PBS, removed from the dishes with 0.25 w/v % Tripsin-1 mmol/L EDTA (WAKO), and collected with PBS. The fluorescent intensity was measured by flow cytometry analysis.

3.4.7. PDT effect of PL-C17 micelles and liposome toward HeLa cells

The phototoxicity of PpIX, PL-C17 micelles, and PL-C17 liposomes toward HeLa cells was examined under light irradiated condition. The cells were incubated for 1-6 h in medium containing various concentrations of PpIX, PL-C17 micelles, or PL-C17 liposomes. After PBS wash, the cells were cultured in RPMI-1640 medium for 0-5 h and irradiated with a xenon lamp (88 mW/cm^2, average) in the 400-800 nm range for 2 min. After incubation for 72 h, cell viability was determined by the MTT assay. In additoion, the defect of cellular membrane of HeLa cells was determined by LDH assay (Cytotoxicity Detection Kit^{PLUS}, Roche).

3.4.8 Reactive oxygen species (ROS) imaging and assay

HeLa cells (5×10^3 cells) were incubated for 1 h in medium containing various concentrations of the PL-C17 micelles and PL-C17 liposomes. Then the cells were cultured in RPMI-1640 medium for 0-5 h and irradiated with a xenon lamp in the 400–800 nm range for 2 min. The cells were stained with 5-(and-6)-chloromethyl-20,70-dichlorodihydrofluorescein diacetate (H2DCFDA; 10 μM, Invitrogen, Carlsbad, CA) for 30 min. The cells were photographed with the microscope after PBS washes. Furthermore, the cells were lysed with 1 % triton X100, and the fluorescent intensity of DCF was determined by a microplate reader.

3.4.9. Detection of oxidation of ROS-induced DOPC

PL-C17 micelle solution (1 mM, 1mL) was added to methanol solution of DOPC (dioleoylphosphatidylcholine, 2.5×10^{-3}mmol) and the mixture was stirred for 1 min. Then, the mixture was irradiated with a xenon lamp (88 mW/cm^2, average) in the 400–800 nm range for 2 min and Mass Spectro of the mixture was measured by LCMS (Shimadzu).

3.4.10. Morphology change of cell-membrane-model liposomes by ROS

Dioleoylphosphatidylcholine (DOPC)-liposomes as cell model were prepared from DOPC, DSPC, Cholesterol and DSPE-PEG (X:1-X:1:0.11, molar ratio; X= 0, 0.1, 0.25, 0.5, 1) by the reverse-phase evaporation (REV) method. [25] Briefly, a mixture of DOPC, DSPC, cholesterol, and DSPE-PEG were dissolved in 5 mL of chloroform/ diisopropylether mixture (1:1, v/v) in a round-bottom flask.100 mM Calcein solution was added to the lipid solution to form an emulsion. The emulsion was sonicated for 3 min., and then, the organic solvent was removed under vacuum in a rotary evaporator at 55 ^{o}C

for 30 min. to obtain a suspension of liposomes. The liposomes obtained were subjected to extrusion 10 times through a polycarbonate membrane of 100 nm pore size (Whatman, 110605, FILTER, 0.1UM, 25MM, Gentaur Molecular Products, Belgium), using an extruder device (LIPEX^{TM} Extruder, Northern Lipids, Canada) thermostated at 55 ºC. Purification was accomplished by ultracentrifuging at 200,000 g for 60 min. at 4 ºC (himaccp 80 wx, Hitachi Koki, Japan), and the pellets obtained were resuspended in saline. PL-C17 micelle solution (10% phospholipid) was added to the liposome solution to generate PL-C17 liposomes (the postinserted liposomes). Purification was accomplished by ultracentrifuging at 200,000 g for 60 min at 4 ºC, and the pellets obtained were resuspended in saline. Particle size of the liposomes were measured with the electrophoretic light scatteringspectrophotometer. The calcein encapsulated DOPC liposome with PL-C17 diluted in 96 well plate. The solution was irradiated were irradiated with a xenon lamp (88 mW/cm^2, average) in the 400-800 nm range for 2 min, then intensity of calcein (Ex=485 nm, Em=525 nm)was measured by fluorescence plate reader (Thermo Fisher). Particle size of calcein encapsulated DOPC liposomes after irradiation were measured with the electrophoretic light scatteringspectrophotometer.

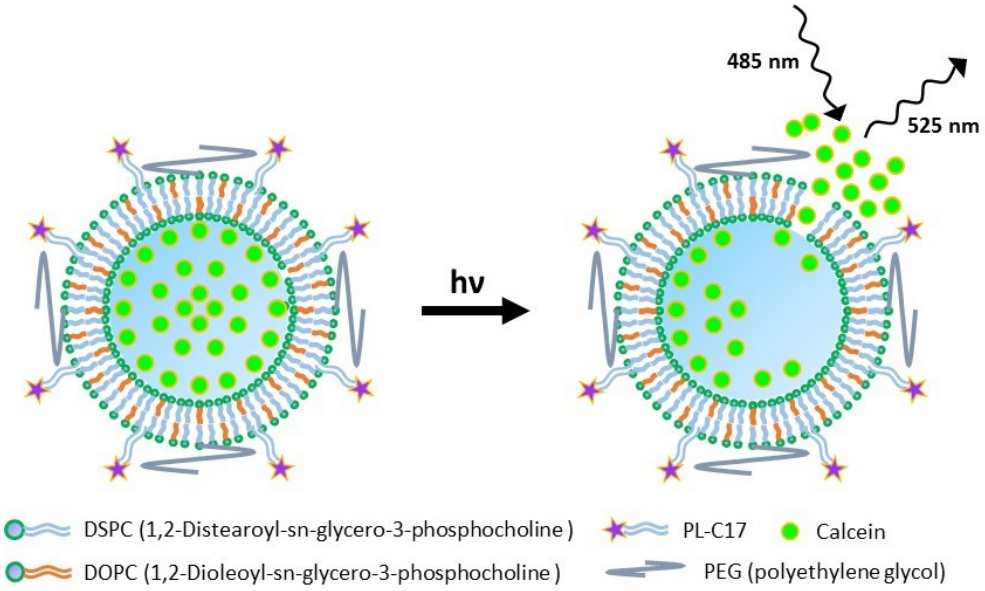

Figure 1. Image of morphology change of cell-membrane-model liposomes composed of 25% DOPC and calcein inner solution

3.4.11. Biodistribution of PL-C17 micelles and liposomes in tumor bearing mice.

Tumor-bearing mice (female, 5-6 weeks old, 16-20 g, Sankyo Labo Service, Japan) were prepared by injecting subcutaneously (s.c.) a suspension (1.0×10^6 cells/mouse) of colon 26 cells directly into the right thigh. The mice were kept on a regular chow diet and water and maintained under 12 h light/dark cycle in an ambient atmosphere. Biodistribution experiments were performed when the tumor diameter was 7 to 9 mm. The tumor-bearing mice were injected via the tail vein with PL-C17 micelles and PL-C17 liposomes (10mg/kg based on PL-C17), or 5-amino-levulinic acid (5-ALA; 9.7 mg/kg)At selected time intervals 5 h (5-ALA) and 36 h (PL-C17 micelles and liposomes) after administration, the mice were lightly anesthetized, sacrificed by cervical dislocation and dissected. The tumor tissue samples were frozen in O.C.T. embedding compoundat -20 ^{o}C, and a cryostat section was prepared for further analysis under a fluorescence microscope (FV100D IX81, OLYMPUS, Japan). After photographed, the tissue section was stained histologically with hematoxylin-eosin (HE). All experiments using mice were performed in compliance with the relevant laws and institutional guidelines approved by the Institutional Animal Care and Use Committee in Gakushuin University.

3.5. References

[1] M.R. Detty, S.L. Gibson, and S.J. Wagner, Current clinical and preclinical photosensitizers for use in photodynamic therapy. *J. Med. Chem.47* (2004) 3897-3915.

[2] D.E. Dolmans, D. Fukumura, and R.K. Jain, Photodynamic therapy for cancer. *Nat. Rev. Cancer 3* (2003) 380-387.

[3] P. Agostinis, K. Berg, K.A. Cengel, T.H. Foster, A.W. Girotti, S.O. Gollnick, S.M. Hahn, M.R. Hamblin, A. Juzeniene, D. Kessel, M. Korbelik, J. Moan, P. Mroz, D. Nowis, J. Piette, B. C. Wilson, and J. Golab, Photodynamic therapy of cancer: An update. *CA Cancer J. Clin.61* (2011) 250-281.

[4] T.J. Dougherty, C.J. Gomer, B.W. Henderson, G. Jori, D. Kessel, M. Korbelik, J. Moan, and Q. Peng, Photodynamic Therapy. *J. Natl. Cancer Inst.90* (1998) 889-905.

[5] A.P. Castano, T.N. Demidova., and M.R. Hamblin, Mechanisms in photodynamic therapy: part two—cellular signaling, cell metabolism and modes of cell death. *Photodiagnosis Photodyn. Ther.2* (2005) 1-23.

[6] J.P. Celli, B.Q. Spring, I. Rizvi, C.L. Evans, K.S. Samkoe, S. Verma, B.W. Pogue, T. Hasan, Imaging and photodynamic therapy: mechanisms, monitoring, and optimization, *Chem. Rev. 110* (2010) 2795–2838.

[7] T.J. Dougherty, W.R. Potter, and K.R. Weishaupt, The Structure of the Active Component of Hematoporphyrin Derivative, in *Porphyrins in Tumor Phototherapy* (Andreoni, A., and Cubeddu, R., Eds.) (1984) 23-35, Springer US.

[8] E.M. Waterfield, M.E. Renke, C.B. Smits, M.D. Gervais, R.D. Bower, M.S. Stonefield, and J.G. Levvy. Wavelength-dependent effects of benzoporphyrin derivative monoacid ring a in vivo and in vitro. *Photochem. Photobiol.60* (1994) 383-387.

[9] T.A. Ciulla, R.P. Danis, M. Criswell, and L.M. Pratt, Changing therapeutic paradigms for exudative age-related macular degeneration: antiangiogenic agents

and photodynamic therapy. *Expert Opinion on Investigational Drugs 8* (1999) 2173-2182.

[10] M.M. el-Sharabasy, A.M. el-Waseef, M.M. Hafez, S.A. Salim, A. Porphyrin metabolism in some malignant diseases. *Br. J. Cancer 65*, (1992) 409-12.

[11] J.C. Kennedy, S.L. Marcus, and R.H. Pottier, Photodynamic therapy (PDT) and photodiagnosis (PD) using endogenous photosensitization induced by 5-aminolevulinic acid (ALA): mechanisms and clinical results. *J. Clin. Laser Med. Surg.14* (1996) 289-304

[12] S. Eleouet, N. Rousset, J. Carre, L. Bourre, V. Vonarx, Y. Lajat, G.M. Beijersbergen van Henegouwen, T. Patrice, In vitro fluorescence, toxicity and phototoxicity induced by delta-aminolevulinic acid (ALA) or ALA-esters, Photochem. *Photobiol. 71* (2000) 447–454.

[13] J.M. Fernandez, M.D. Bilgin, L.I. Grossweiner, Singlet oxygen generation by photodynamic agents, *J. Photochem. Photobiol., B 37* (1997) 131–140.

[14] Y.Y. Huang, S.K. Sharma, T. Dai, H. Chung, A. Yaroslavsky, M. Garcia-Diaz, J. Chang, L. Y. Chiang, M. R. Hamblin, *Nanotech. Rev. 1* (2012) 111.

[15] S. Battah, S. Balaratnam, A. Casas, S. O'Neill, C. Edwards, A. Batlle, P. Dobbin, A.J.MacRobert, Macromolecular delivery of 5-aminolaevulinic acid for photodynamic therapy using dendrimer conjugates, *Mol. Cancer Ther. 6* (2007) 876–885.

[16] C.J. Rijcken, J.W. Hofman, F. van Zeeland, W.E. Hennink, C.F. van Nostrum Photosensitiser-loaded biodegradable polymeric micelles: preparation, characterisationand in vitro PDT efficacy, *J. C. R. 124* (2007) 144–153.

[17] A.M. Master, M.E. Rodriguez, M.E. Kenney, N.L. Oleinick, A.S. Gupta, Delivery of the photosensitizer Pc 4 in PEG-PCL micelles for in vitro PDT studies, *J. Pharm. Sci. 99* (2010) 2386–2398

[18] J.F. Lovell, C.S. Jin, E. Huynh, H. Jin, C. Kim, J. L. Rubinstein, W.C. Chan, W. Cao, L. V. Wang, and G. Zheng, Porphysome nanovesicles generated by porphyrin bilayers for use as multimodal biophotonic contrast agents. *Nature materials 10*

(2011) 324-32.

[19] E. Huynh, J.F. Lovell, B.L. Helfield, M. Jeon, C. Kim, D.E. Goertz, B.C. Wilson, and G. Zheng, Porphyrin shell microbubbles with intrinsic ultrasound and photoacoustic properties. *J. Am. Chem. Soc.134* (2012) 16464-16467.

[20] G.I. Lozovaya, Z. Masinovsky, A.A. Sivash, Protoporphyrin IX as a possible ancient photosensitizer : spectral and photochemical *Orig. Life Evol. Biosph*. *20* (1990) 321-330

[21] L.M. Scolaro, M. Castriciano, A. Romeo, S. Patane, E. Cefali, M. Allegrini, Aggregation Behavior of Protoporphyrin IX in Aqueous Solutions: Clear Evidence of Vesicle Formation *J.Phys. Chem. B* 106 (2002) 2453-2459.

[22] M. Price, N. Okan-Mensah, A.M. Santiago, and D. Kessel, D The role of reactive oxygen species in PDT efficacy, (2009)

[23] E. Engel, R. Schraml, T. Maisch, K. Kobuch, B. König, R. M. Szeimies, J. Hillenkamp, W. Bäumler and R. Vasold Light-Induced decomposition of Indocyanine Green *IVOS*, May 49, (2008) 1777-1783

[24] M.E. El-Zaria, H.S. Ban, and H. Nakamura, Boron-Containing Protoporphyrin IX Derivatives and Their Modification for Boron Neutron Capture Therapy: Synthesis, Characterization, and Comparative In Vitro Toxicity Evaluation. *Chem. Eur. J. 16* (2010) 1543-1552.

[25] F.J. Szoka, and D. Papahadjopoulos, Procedure for preparation of liposomes with large internal aqueous space and high capture by reverse-phase evaporation. *Proc. Natl. Acad. Sci. U. S. A. 75*, (1978) 4194-4198.

Conclusion

Recentry, cancer treatment has dramatically changed. Development of a noninvasive therapy is now emerging requirement in terms of quality of life (QOL) for cancer patients. In this regards, I focused on BNCT and PDT and studied the development of new therapeutic agents based on the technology of liposomal drug delivery system. Drug delivery systems (DDS) is delivery of drugs using nanocarrier to target sites selectivery, liposome can be used as drug carriers for improving the delivery of therapeutic agents.

The successful treatment of cancer patients by BNCT relies on the selective delivery of ^{10}B to tumor cells and its high accumulation therein. Therefore, the development of high ^{10}B content liposomes is necessary for clinical use. In this work, we studied the effects of the counter cations of boron clusters for the liposome formation. We were able to develop high boron content liposomes for BNCT by overcoming osmotic pressure limitations. The use of spermidiniumcation (spd) as an alternative counter cation of *closo*-dodecaborates was essential for the preparation of high boron content liposome solutions; final boron concentration in the liposome solutions was approximately 14,000 ppm and B/P ratio was 3.5. The spd cation prevented the interaction of anionic *closo*-dodecaborates ($[B_{12}H_{12}]^{2-}$) with the phosphatidylcholine moiety of 1,2-distearoyl-sn-glycero-3-phosphocholine (DSPC) in the liposomes, thereby suppressing the release of liposome contents and increasing liposome yield. Tumor boron concentrations reached 203 and 242 ppm 36 h after injecting colon 26 tumor bearing mice with 100 mg B/kg of spd-$[B_{12}H_{11}SH]$ and spd-$[B_{12}H_{11}NH_3]$ encapsulating liposomes, respectively. Tumor boron concentrations of 34.0 and 35.4 ppm were noted 36 h after injecting 15 mg B/kg of spd-$[B_{12}H_{11}SH]$- and spd-$[B_{12}H_{11}NH_3]$- encapsulating liposomes, respectively. Significant antitumor effect was observed in mice that received a single injection. The tumor completely disappeared three weeks after thermal neutron irradiation ($(1.5-1.8) \times 10^{12}$ neutrons/cm^2) and was locally controlled for 100 days after the irradiation even at the dose of 15 mg B/kg. The total amount of liposomes was reduced to less than one-seventh of the amount of liposomes used to prepare Na_2BSH-encapsulating liposomes. We believe that the spd-

closo- dodecaborate-encapsulating liposomes are a promising candidate for clinical use in BNCT.

Also, the successful treatment of PDT relies on the selective delivery of photosensitizer to tumor tissue. Therefore, we synthesized PpIX lipid (PL) attaching two long alkyl chain, such as C13, C15, and C17, on PpIX. The PpIX lipids having amphiphilic property exhibited a water solubility by forming their micelle formations in water and relatively low cytotoxicity toward HeLa cells without light irradiation. PL-C17 liposomes were readily prepared by post-insertion of PL-C17 into outer membrane of the liposomes. Also, PL-C17 micelle homogeneously-dispersed on membrane of the liposomes prevent the aggregation of porphyrins that is considered to diminish the PDT effect. These PL-C17 micellles, liposome and PpIX distributed evenly in the membrane and cytoplasm of cells treated with each porphyrin at 100 μM concentration for 1 h. However, PL-C17 micelles and liposome translated to Golgi after 2h and to a certain organelle in the cells after 5 h, whereas PpIX remained in the membrane and cytoplasm. Furthermore, PDT effect of each porphyrin derivative on HeLa cells was highly dependent on the intracellular localization. A significant cytotoxicity was observed in the porphyrin derivatives localized in plasma membrane, whereas low cytotoxicity was observed in the porphyrin derivatives accumulated into the cytoplasm. In order to clarify the mechanism of phototoxicity, we examined the LDH assay to analyze cellular membrane defect. Cytopathic damage of the cell membrane is highly dependent on the localization of porphyrin derivatives. Furthermore, the intracellular ROS generation was detected by molecular green fluorescent probe CM-H_2DCFDA, revealing that the localization of porpyrin derivatives is more important than the accumulation for the PDT effect on HeLa cells. Indeed, the experiment using calcein-encapsulating DOPC liposome with PL-C17 for the cell membrane model suggested the possibility of phototoxicity caused by disruption of cellular membrane by the oxidation of unsaturated phospholipids by ROS.

Finally, PL-C17 liposomes were observed in tumor tissue 36 h after *i.v.* administration in tumor-bearing mice. Since PL-C17 liposomes are still vacant in their interior aqueous core, drugs including photosensitizers or antitumor agents are able to be encapsulated in

the liposomes. In this regard, we can envision the combination therapy of PDT and chemotherapy using the current photosensitizer lipid liposome system.

Acknowledgment

The research described in this doctoral dissertation has been carried out at the Graduate School of Science, Gakushuin University.

First of all, I would like to express my deepest gratitude to Professor Fumio Hanaoka for his encouragement, continuous guidance and valuable suggestions throughout the course of this work.

I would like to thanks to Professor Takashi Hishida, Professor Hiroyuki Nakamura and Professor Nobuhiro Nishiyama for their carefully proofreading and suggestions.

I am thankful to Professor Koji Ono and Professor Minoru Suzuki for providing a good opportunity for neutron irradiation experiment at Kyoto University Research Reactor Institute.

Finally, I express my deepest gratitude to my close friend and collaborator who taught me the good things that really matter in life.

Shinichi Sato, Ph.D., Masayuki Yokoi, Ph.D., Mohamed E. El-Zaria, Ph.D., Masaharu Uno, Ph.D., Hideyuki Nakayama, Ph.D., Shinichi Kojima, Ph.D., Hidekazu Arii, Ph.D., Hyun Seung Ban, Ph.D., Akihisa Aimi, Ph.D., Hidemitsu Minegishi, Ph.D., Mr. Wataru Nabeyama, Mr. Ryu Inomata, Mr. Taturo Miyoshi, Mr. Hayato Koganei, Mr. Shinji Fukashiro, Mr. Daisuke Kanoh, Mr. Shunsuke Kikuchi, Tubasa Watanabe, M.D., Mr. Yasuaki Taira, Mr. Yuji Shimokawa, Mr. Masaya Kurihara, Ms. Erina Suzuki

Thanks for their help, their kindness, and useful suggestions.

本研究が、いつか、どこかで、だれかの、役に立つことができたならば、
その時初めて、喜びと安堵を、少しだけ誇りを持つことができる